

Variation analysis of multiple tsunami inundation models

Yoshinori Shigihara ^a, Kentaro Imai ^b, Hiroyuki Iwase^c, Koji Kawasaki^d, Makoto Nemoto^e, Toshitaka Baba^f, Naotaka Yamamoto Chikasada ^g, Yu Chida^h and Taro Arikawa ⁱ

^aDepartment of Civil and Environmental Engineering, National Defense Academy, Yokosuka, Japan; ^bResearch Institute for Marine Geodynamics, Japan Agency for Marine-Earth Science and Technology, Yokohama, Japan; ^cFirst Investigation & Research Department, The Japanese Institute of Fisheries Infrastructure and Communities, Tokyo, Japan; ^dR&D Center, Hydro Technology Institute Co, Ltd, Osaka, Japan (Department of Civil Engineering, Meijo University, Nagoya, Japan); ^eEarthquake Risk Management Division, OYO Corporation, Saitama, Japan; ^fGraduate School of Technology, Industrial and Social Sciences, Tokushima University, Tokushima, Japan; ^gEarthquake and Tsunami Research Division, National Research Institute for Earth Science and Disaster Resilience, Tsukuba, Japan; ^hTsunami and Storm Surge Group, Port and Airport Research Institute, Yokosuka, Japan; ⁱFaculty of Science and Engineering, Civil and Environmental Engineering, Chuo University, Tokyo, Japan

ABSTRACT

Researchers have developed tsunami inundation models based on nonlinear shallow water equations to estimate tsunami propagation and inundation. However, their empirical results are not in perfect agreement with those of other research institutes, even though the same governing equations are used. Therefore, we quantitatively evaluated the variability of tsunami simulations in this study. Several research institutes have conducted tsunami simulations under the same input conditions using tsunami inundation models adopted for tsunami hazard assessment, resulting in a certain degree of variability among them. By examining the spatial and temporal differences in various physical quantities, we identified the characteristic topography where the variability between tsunami simulations increases. A novel method for calculating statistics from the area integrals of physical quantities was proposed to demonstrate the variability in the overall simulation results. In addition, the effects of different setting parameters and computational environments on the simulation results of a single model were evaluated. The findings of this study are expected to not only serve as a basis to verify the reliability of source codes employed by users of the tsunami inundation model, but also contribute useful technical information to advance probabilistic tsunami hazard assessment in the future.

ARTICLE HISTORY

Received 11 May 2021
Accepted 4 October 2021

KEYWORDS

Tsunami; tsunami inundation model; multiple model comparison; variation analysis

1. Introduction

Structural measures such as coastal dikes and breakwaters, and non-structural measures such as tsunami hazard maps and evacuation information systems have been developed to prevent tsunami damage. To utilize these measures effectively, it is important to predict tsunami damage using numerical simulations. Examples of numerical models to predict tsunami damage include ALASKA (Kowalik and Murty 1993; Nicolsky, Suleimani, and Hansen 2011), FUNWAVE-TVD (Shi et al. 2012), GeoClaw (George and LeVeque 2006; George 2008), JAGURS (Baba et al. 2014), MOST (Titov and Synolakis 1995, 1998), NEOWAVE (Kowalik et al. 2005; Yamazaki, Kowalik, and Cheng 2008), TNS (Miyoshi et al. 2019), T-STOC (Tomita and Kakinuma 2005; Tomita, Honda, and Chida 2016), TUNAMI-N1 (Shuto, Goto, and Imamura 1990; Goto and Ogawa 1997), and TUNAMI-N2 (Imamura 1995; Imamura, Yalciner, and Ozyurt 2006). These models can evaluate tsunami generation and propagation and the inundation of land. The source code of some of the models is available free of charge.

In general, numerical models must be developed to guarantee the accuracy and reliability of the results. In a numerical tsunami model, numerical solutions are compared with analytical solutions, hydraulic experimental data, and observation data obtained from actual past tsunami events. If the error between the numerical solution and observation data is confirmed to be within a certain range, the model can be used for tsunami hazard-mapping projects. In the United States, the National Tsunami Hazard Mitigation Program holds regular workshops on the accuracy verification of numerical tsunami models, and the results are reported periodically (e.g. Horrillo et al. 2015; Lynett et al. 2017). Moreover, the analytical solutions adopted in the workshops and data from hydraulic experiments have been made available as benchmark problems. In a similar effort, the Japan Society of Civil Engineers (JSCE) held a tsunami analysis hackathon in September 2020. The purpose of the hackathon was to develop and improve numerical models by comparing them with hydraulic experimental data to improve tsunami numerical analysis techniques. The hackathon focused not only on tsunami propagation and

inundation problems, but also on the evaluation of tsunami wave pressure and the forces acting on structures, and the phenomena associated with tsunami flow, such as changes in the seafloor topography due to sediment transport and the behavior of drifting objects. These results are reported by Yasuda et al. (2021), Yamamoto et al. (2021), and Takabatake et al. (2021). Furthermore, the hydraulic experiment data adopted in the hackathon are available on the tsunami disaster prevention portal site (JSCE and NIED 2018). Tide records from offshore tsunami gauges are often used to validate a model by comparison with observed data (e.g. Titov 2009). As an example of coastal tsunami run-up and inundation data, the trace height distribution for Okushiri Island during the 1993 Hokkaido Nansei-Oki Earthquake Tsunami was published as a benchmark problem (Takahashi 1996). In the 2011 earthquake and tsunami off the Pacific coast of Tohoku, a large amount of observation data on tsunamis was obtained over a wide area. Hayashi and Koshimura (2013) and Montoya et al. (2016) used measured data such as the inundation height distribution on land and flow velocity analyzed in video images of the Sendai Plain to verify the accuracy of tsunami inundation models (TUNAMI for the former, MOST and GeoClaw for the latter).

To run a simulation using a tsunami inundation model whose accuracy has been guaranteed through the above process, it is necessary to set up various computational conditions, including the grid generation of the computational domain. In some research fields, the complexity of these pre- and post-processing steps makes it difficult to perform the simulation. It is relatively easy to obtain input data for tsunami simulations in Japan. Information about the fault parameters in the sea areas around Japan is publicly available for the crustal deformation of earthquakes, which are the source of tsunamis. Similarly, topography data are available at multiple resolutions, along with land use classification data and data on structures such as coastal dikes and submerged breakwaters. In addition, there are many commercial and free software packages for visualizing the simulation results. To conduct tsunami simulations using the input data described above, we can refer to the procedures described in the guidelines established for the target facilities (e.g. MLIT 2012; JSCE 2016, the former is for municipalities and the latter is for nuclear power plants). In this way, we can make tsunami simulations available to everyone.

On the contrary, the users of the numerical tsunami models have found that the results of their tsunami simulations do not completely agree with those of other institutes, even if they use the same governing equations, computational methods, and condition settings. This can be understood as epistemic uncertainty

owing to the facts that the parameters used in the code, such as the lower limit of the flow depth at the tip of the tsunami and upper limit of the flow velocity, are set independently by each research institute, and that there are differences in the methods of processing the input and output data and in the computing environments used, such as the computers and compilers, even though the same source code is used. Because the occurrence of this type of uncertainty is caused by a lack of knowledge or information about the numerical model itself, or by the system, such as the parameters used in the numerical model (Hoffman and Hammonds 1994), it is possible to reduce this uncertainty by accumulating scientific knowledge. Therefore, it is extremely important to quantitatively evaluate where and how much variability exists by comparing multiple simulation results, and to clarify factors such as how much variability is caused by differences in parameter settings and computational environments to reduce the uncertainty of numerical models. In recent years, it has been demonstrated that the probabilistic tsunami hazard assessment (PTHA), which takes into account various uncertainties, is necessary for the risk assessment of critical facilities located in coastal areas such as nuclear power plants and, in the case of Japan, Self-Defense Force bases (JSCE 2016). In general, the uncertainty in PTHA is considered for the fault parameters of earthquakes in the tsunami generated area (e.g. Fukutani et al. 2021). However, to propose a more explanatory PTHA in the future, the uncertainty caused by the numerical models in the tsunami propagation and run-up processes must be considered, but at present, must be given empirically.

In this study, we attempted to clarify the differences in the simulation results generated by the standard tsunami inundation models currently used in practice and to quantitatively evaluate the variations between them. Several tsunami simulations were carried out with the same input data, such as bathymetry data, land topography data, and tsunami source models, and the results were compared. Several research institutes that use numerical tsunami models for tsunami hazard mapping and tsunami damage estimation participated in this project. The differences in various physical quantities, such as water surface levels and flow velocities obtained from the tsunami simulations by each organization were investigated spatially and temporally, and the areas where the variations are especially large were analyzed, along with their characteristics. Furthermore, we proposed a comparison method using the integration of physical quantities to show the magnitude of the variation in the simulation results. We not only compared the variability among the numerical tsunami models of the institutes included in this study, but also examined that calculated by varying the setting parameters of a specific

model under multiple conditions in different computing environments. Clarifying the existence and characteristics of the variability generated by tsunami simulations and quantitatively evaluating its magnitude is expected to not only serve as a standard for verifying the reliability of source codes employed by users of tsunami inundation models, but also contribute useful information to the technological development of PTHA.

Note that the purpose of this study was to compare the relative performance of the models and not to evaluate their validity or to determine their superiority or inferiority. The models selected for comparison are based on the shallow water (nonlinear long-wave theory) equations currently used as a standard in tsunami disaster prevention work in Japan. Their accuracy has already been verified by comparison with hydraulic experimental data (Yasuda et al. 2021).

2. Methods

In this section, the details of the input data and computational conditions used in the tsunami simulation and the numerical models compared are presented. To extract the differences between the tsunami inundation models due to the differences in physical and numerical conditions, it is important to minimize the uncertainty of the setting conditions. For this purpose, it was desirable to prepare an environment where modelers could use the same topography model and initial conditions (tsunami source models). Therefore, we decided to use publicly available and easily accessible data on hypothetical tsunami events to compare the models. The details are presented below.

2.1. Bathymetry and topography data

In Japan, datasets have been developed for each region where earthquake and tsunami damage predictions are carried out, and they have been deposited at the G-Spatial Information Center (AIGID 2016). We used the dataset from “the Massive Earthquake Model Review Meeting of the Nankai Trough” (Cabinet Office 2012). The datasets, which include tsunami source models and bathymetry and land topography data, can be downloaded free of charge.

(Figure 1) illustrates the 2430-m-resolution (covering the western part of Japan from the Kanto region) and the 90-m-resolution grid domain (covering the vicinity of Kochi Prefecture) used in the simulation. The bathymetry and land topography data consist of six levels, with spatial resolutions ranging from 2430 m to 10 m, and provide information about the spatial connectivity between regions for multiple geographic coordinate systems. In this study, we used the dataset in the plane-rectangular coordinate system zone no. 4; the 10 m grid domain, which has the smallest spatial

resolution, was evaluated for two locations, Kochi City and Susaki City, in Kochi Prefecture (Figure 2). This is to investigate the differences in the results due to the topography of low-lying areas and the ria coast. The above descriptions are summarized in (Table 1). The area number in the table corresponds to the file number of the dataset.

2.2. Tsunami source model

In the tsunami source model, there are 11 fault models that were developed for the Nankai Trough mega earthquake. Among them, we used Case 4, which has a large fault slip off the Shikoku region (see Figure 1 for details of the crustal deformation). Normally, for a magnitude 9 earthquake, the effects of dynamic fault rupture, that is, rupture speed and rise time, should be considered. For the sake of simplicity, we did not take them into account and set them so that the permanent displacement was reached the moment the earthquake occurred. The dataset contains crustal deformation (i.e. initial water surface level distribution) precomputed by the fault parameters of the earthquake. (The spatial grid spacing was computed at an 810 m resolution). We used these data as a basis for generating crustal deformation data for other spatial resolutions. The interpolation method used was arbitrary.

2.3. Other conditions

The other setting conditions are based on the guideline “Guide to Determining the Potential Tsunami Inundation” by the Ministry of Land, Infrastructure, Transport and Tourism (MLIT 2012). Only subsidence was considered in the setting of crustal deformation of the land area. All areas of Kochi City and Susaki City, which are the target areas of the simulation, are subject to subsidence, and the ground level is lower than the sea level in some areas. An identifier to discriminate between sea and land was created in advance and given as input data to enable verification of whether such areas are inundated or not. The effect of resistance by structures was considered as the bottom friction force by assigning Manning’s roughness coefficient according to the land use by Kotani, Imamura, and Shuto (1998). This method is recognized as a standard model in the above guidelines, and the matrix data are included in the dataset provided by the Cabinet Office; we used those data. Furthermore, structures such as rivers and coastal dikes, breakwaters, and submerged dikes are usually defined on the boundary of the grid to apply the overtopping condition; however, in this study, these structures were assumed to be nonfunctional (i.e. not considered) because they are destroyed in the worst-case scenario. The tide level was set at T.P. (Tokyo Peil) 0 m as a constant value.

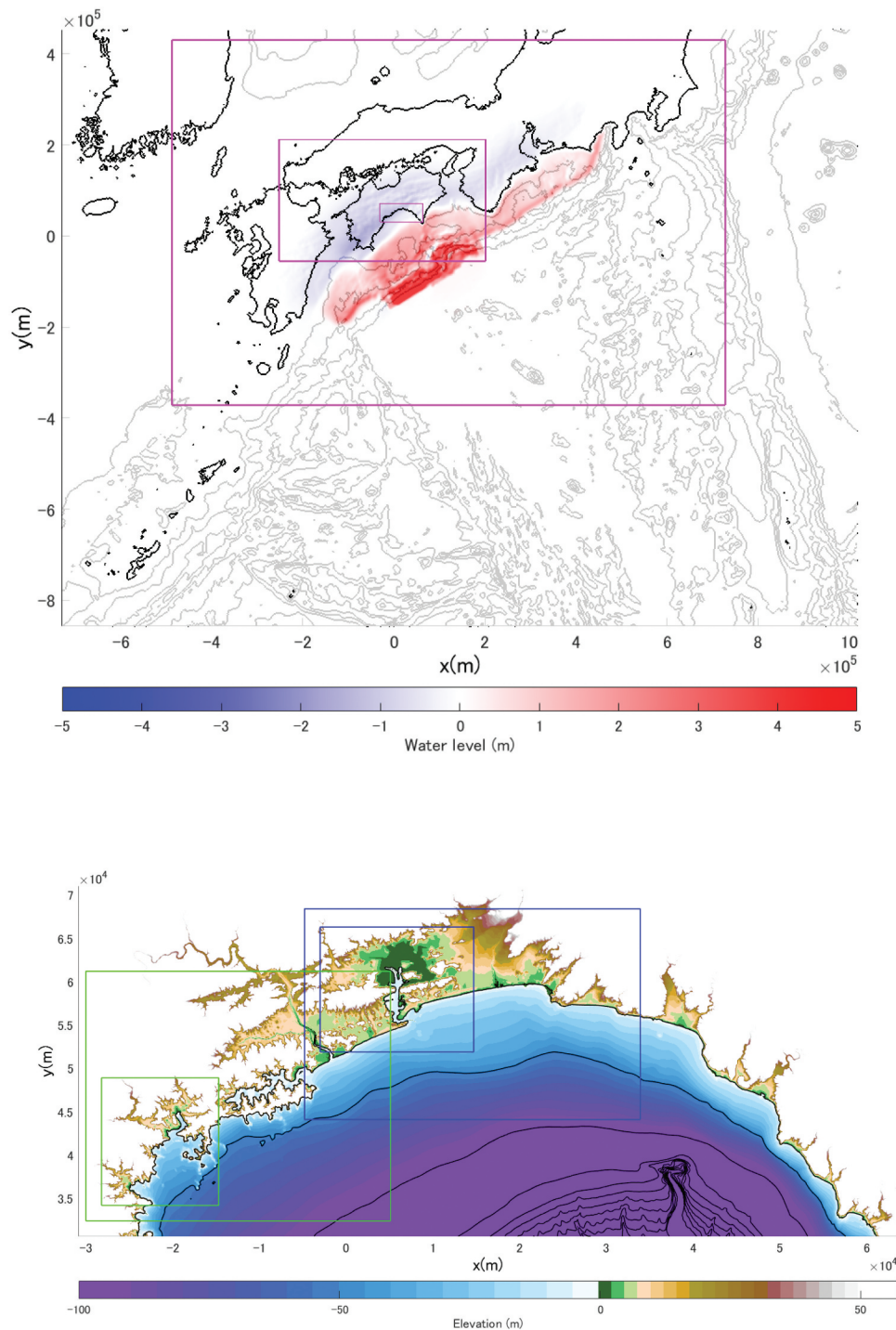


Figure 1. Computational domain. Upper panel: seafloor displacement in 2430 m grid domain (i.e. initial water surface level distribution of a tsunami). The square boxes indicate the 810 m, 270 m, and 90 m grid domain, respectively. Lower panel: Distribution of bathymetry and topography on a 90 m grid. The square boxes indicate the range of the 30 m and 10 m grid domain, respectively.

2.4. Tsunami inundation models and computational conditions

Using the input data described thus far, the results of the simulations using several numerical tsunami models were compared. In this study, TUNAMI(-N1, -N2, and TNS) and JAGURS, validated by Yasuda et al. (2021) as described above, were used. Specifically, in the tsunami analysis hackathon, the results of tsunami inundation experiments were

compared with numerical model reproductions using an urban model that reconstructed the detailed topography of Onagawa Town, damaged by the 2011 Tohoku Tsunami. The results indicated that TUNAMI and JAGURS could reproduce the tsunami inundation phenomena with an average accuracy of approximately 90% for several maximum tsunami water levels measured using water level gauges.

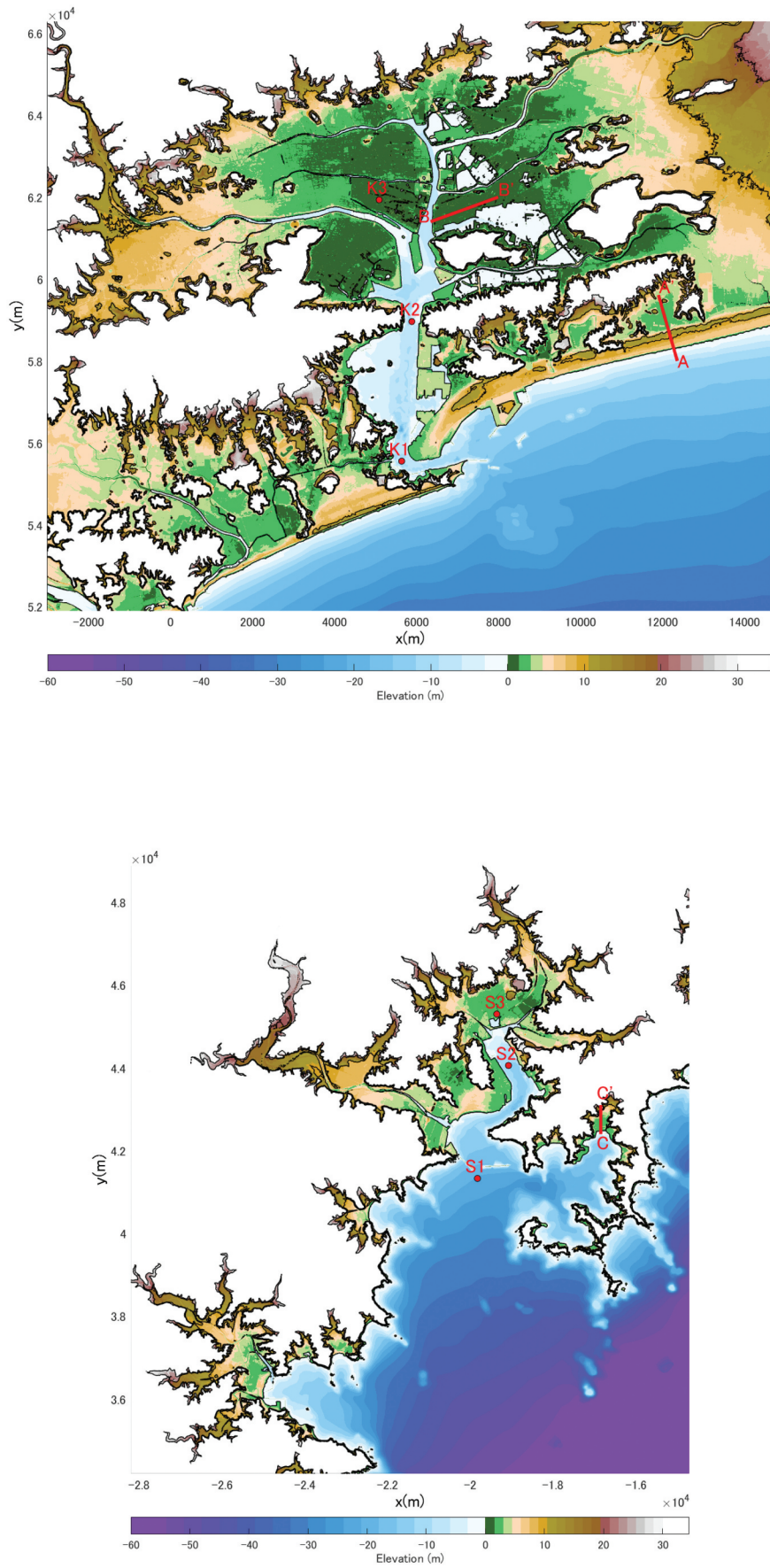


Figure 2. Distribution of bathymetry and topography on 10 m grid domain. Upper panel: Kochi City, Lower panel: Susaki City.

Table 1. Information of bathymetry data used.

Area #	Grid size[m]	Matrix size (imax × jmax)	Location of the southwest corner ^b [m]		Note
			x	y	
2430-01	2430	720 × 540	-730,200	-857,700	
0810-01	810	1500 × 990	-487,200	-371,700	
0270-01	270	1680 × 990	-252,300	-55,800	
0090-03	90	1050 × 450	-30,900	30,600	
0030-08	30	1170 × 960	-30,000	32,400	for Susaki City
0030-09	30	1290 × 810	-4800	44,100	for Kochi City
0010-17	10	1350 × 1470	-28,200	34,200	for Susaki City
0010-19	10	1770 × 1440	-3000	51,900	for Kochi City

^aimax and jmax are the maximum number of grids in the east-west and north-south directions, respectively.

^bThese locations indicate the origin of each domain, and the coordinates are based on Zone 4 of the rectangular plane, where x and y are east-west and north-south directions are indicated.

The governing equations are based on nonlinear shallow water equations (or nonlinear long-wave theory) with conservative and hydrostatic-type models. The continuity and motion equations are expressed as follows:

$$\frac{\partial \eta}{\partial t} + \frac{\partial M}{\partial x} + \frac{\partial N}{\partial y} = 0 \quad (1)$$

$$\begin{aligned} \frac{\partial M}{\partial t} + \frac{\partial}{\partial x} \left(\frac{M^2}{D} \right) + \frac{\partial}{\partial y} \left(\frac{MN}{D} \right) \\ = -gD \frac{\partial \eta}{\partial x} - \frac{gn^2}{D^{7/3}} M \sqrt{M^2 + N^2} \end{aligned} \quad (2)$$

$$\begin{aligned} \frac{\partial N}{\partial t} + \frac{\partial}{\partial x} \left(\frac{MN}{D} \right) + \frac{\partial}{\partial y} \left(\frac{N^2}{D} \right) \\ = -gD \frac{\partial \eta}{\partial y} - \frac{gn^2}{D^{7/3}} N \sqrt{M^2 + N^2} \end{aligned} \quad (3)$$

where η is the water surface level; M and N are the line discharge rates in the x and y directions, respectively; h is the still water depth; D is the total water depth ($= h + \eta$); g is the acceleration due to gravity; and n is Manning's roughness coefficient. In recent years,

non-hydrostatic models based on dispersive wave theory have been developed as models with higher-order accuracy (e.g. Iwase and Imamura 2004; Shigihara and Fujima 2006, 2014; Baba et al. 2015). In addition, a model incorporating the loading effects and vertical density distribution of seawater (e.g. Baba et al. 2017) has been proposed to improve the reproduction of far-field tsunamis. However, the above four models were used to study the differences in the numerical models of nonlinear long-wave theory, which is commonly used in practical simulations such as the tsunami hazard assessments currently conducted in Japan.

(Table 2) lists the details and computational conditions of each tsunami inundation model. All the models use a finite difference scheme based on the staggered leapfrog method, where the advection term is the first-order accurate upwind difference, and the linear term is the second-order accurate central difference. The difference between the models is the condition at the tsunami front (moving boundary condition). One of the following models is used: Iwasaki and Mano (1979), Imamura (1996), or a modified model of Imamura (1996) (see Imamura (2009) for the details of each method). The nesting method of the spatial grid, the coordinate system, and the conditions for the minimum time step and reproduction time are assumed to be identical. Six research institutes participated in this project. Each institute used one of the four models and was allowed to set any value for the parameters used in the simulation. In general, when running numerical tsunami models, it is necessary to provide several parameters, such as the upper limit of the flow velocity and the minimum water depth at the tsunami front (wet/dry condition), and the differences in these settings are expected to affect the simulation results. However, there are few references that provide specific recommended values for these parameters, and only MLIT (2012) clearly states that "the minimum value of the flow depth at the tsunami front should be approximately 0.01 m." Therefore, the values of the parameters are set by the organizations that develop the tsunami inundation models, but in some cases, the users provide their own parameters empirically.

Table 2. Summary of model used and common conditions for the simulation.

Model name	Governing equation	Numerical accuracy of linear terms	Numerical treatment of convection term	Moving boundary condition
TUNAMI-N1	Nonlinear shallow water equations (hydrostatic model, Conservative type)	Staggered Leap-Frog (2nd-order accurate)	Upwind (1st-order accurate)	Iwasaki & Mano(1979)
TUNAMI-N2				Imamura (1996)
TNS				Imamura (1996)
JAGRUS				Imamura (1996) ^a
Model name	Coordinate system	Spatial grid size and nesting system	Time step [sec]	Total simulation time [hrs]
TUNAMI-N1	Cartesian (Rectangular) coordinates	Two-way, 6-levels (2430, 810, 270, 90, 30, 10 m)	0.2	12
TUNAMI-N2				
TNS				
JAGRUS				

^aOnly pressure gradients are considered in the scheme.

Table 3. Summary of physical and numerical conditions for the simulation.

Model #	Grid nesting for time	Limit of maximum flow velocity [m/s] ^a	Minimum flow depth for dry-wet condition [m]	Minimum flow depth for bottom friction terms [m]
1	No	7	1.0E-05	1.0E-05
2	No	7	1.0E-05	1.0E-05
3	Yes	50	1.0E-05	1.0E-02
4	No	20	1.0E-05	1.0E-02
5	Yes	10	1.0E-05	1.0E-05
6	No	$Fr = 2$	1.0E-06	1.0E-06

Model #	Gravity acceleration [m/s ²]	Numeric precision	Compiler	Parallelization
1	9.8	Single	Intel Fortran Composer XE 15.0	No
2	9.8	Single	Intel Fortran Compiler Professional 11.1	No
3	9.8	Single	Intel Fortran Composer XE 14.0	No
4	9.80665	Double	Intel Fortran Linux 13.1	OpenMP
5	9.8	Single	NVIDIA Cuda compiler 7.5	CUDA
6	9.8	Double	Intel Fortran Composer XE 14.0	OpenMP+MPI

^a Fr represents the Froude number.

The values of the parameters used by each participant are listed in (Table 3). Note that only the parameters common to all models are shown here; there may be other parameters used by individual users. In this table, in addition to the parameters, the presence or absence of time nesting, type of real numbers used (single or double precision), type of compiler, and computing environment are also described. All the models are written in Fortran 77 or 90, and some of them have been used in practical applications for large-scale computation with the use of parallelization (e.g. Oishi, Imamura, and Sugawara 2015; Baba et al. 2016).

3. Spatio-temporal characteristics of the variability of simulation results generated from multiple tsunami inundation models

The simulation results obtained by each research institute were analyzed based on the computational conditions and methods described in the previous section. In this section, we first compare the temporal changes

Table 4. Information on the output points for water surface level and velocity and the start and end points of transect of the geophysical quantity distribution.

Name	Location ^a [m]		Ground elevation at output point ^b [m]
	x	y	
K1	55,554	5644	-9.91
K2	58,963	5892	-7.11
K3	61,934	5095	-1.33
S1	41,328	-19,825	-23.1
S2	44,057	-19,075	-13.2
S3	45,297	-19,358	0.71

Name	Start point[m]		End point[m]	
	x	y	x	y
A-A'	12,370	58,000	11,910	59,610
R-R'	6350	61,400	8000	62,000
C-C'	-16,845	42,400	-16,845	43,100

^ax and y represent the east-west and north-south directions, respectively, and are based on Zone 4 of the plane rectangular coordinate system.

^bThe ground elevation is based on T.P. Points K3 and S3 are heights on land, and the other points are water depths.

in the water surface level and flow velocity at several representative points. Next, the statistics obtained from the spatial distribution of the maximum values of the tsunami physical parameters (water surface level, flow depth, velocity, and momentum flux) are compared. Then, we identify the region where the variability among the tsunami inundation models of the physical quantities increases, and clarify the characteristics of the variability.

3.1. Time variation of water surface level, flow depth, and flow velocity

First, the temporal changes in the water surface level and flow velocity were compared. The output points are shown in (Figure 2) and listed in (Table 4). Three locations from the sea to the land were selected in Kochi City and Susaki City, respectively. (Figures 3 and 4) depict the results of superimposing all the models on the time series of each point. The overall trend is that the temporal changes are quite similar, and all the models provide comparable numerical solutions. However, there were some local differences that cannot be ignored.

At K1, located at the mouth of Urado Bay, the peak velocity of the first wave is approximately 6–9 m/s, which represents approximately a 30% difference between the models. The topography of the site is complex, with a large curvature caused by sandbars protruding in the east-west direction. At S1 in Susaki Bay, there is a large difference in the flow velocity, especially when a backwash occurs. The reason for this difference is that point S1 is located on the open sea side of the breakwater at the mouth of the bay, where the current is strong and the velocity is extremely high. Thus, in the area where the topography changes markedly, the water surface level changes significantly, and the corresponding difference in flow velocity also increases.

Contrarily, the differences in the maximum and minimum peak values at K2 and S2, located farther inland, are quite small, although phase shifts occur

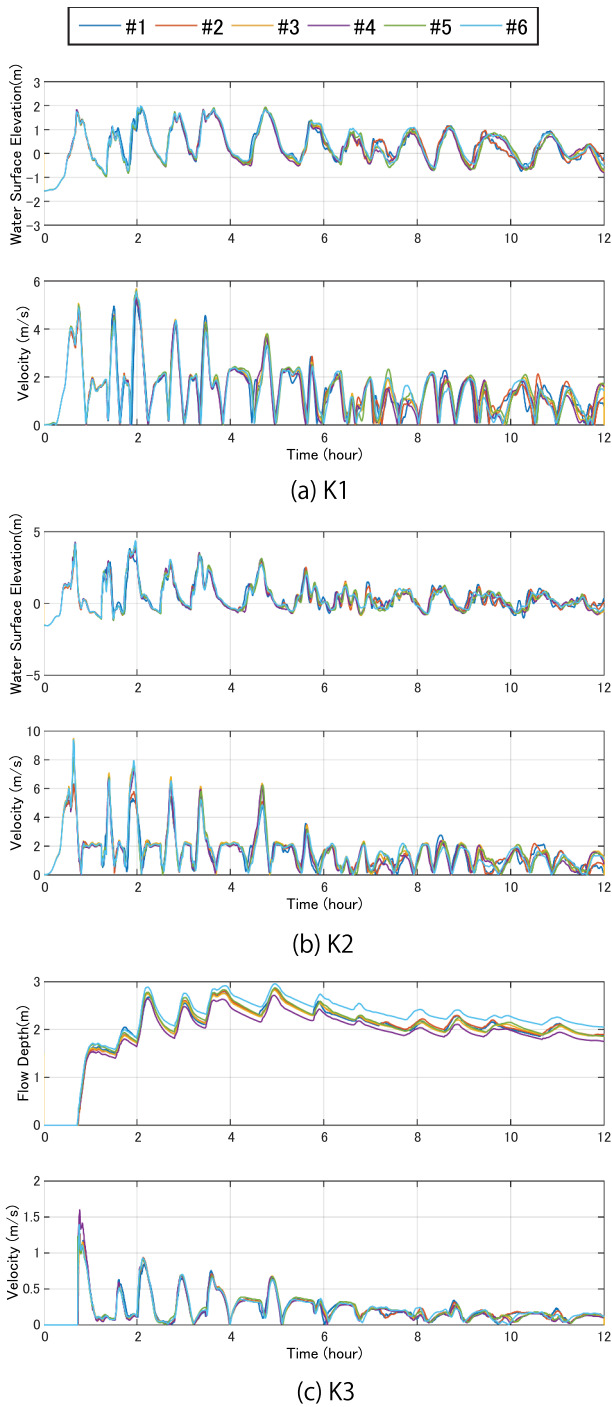


Figure 3. Time series of water surface Elevation, flow depth and flow velocity at the locations shown in Figure 2. The color of the lines in the figures corresponds to the model # in the legend placed on top of the panels.

over time. The temporal variation in the flow depth in K3 was similar, but the overall difference was approximately several tens of centimeters, and the peak velocity at the time of tsunami arrival differed by approximately 20%. The nonlinear effect is especially large for the run-up phenomenon of tsunamis on land. Therefore, it appears that differences in the use of advection terms between the models and in the processing of the output as cross-sectional mean flow velocity were the cause of the differences in the simulations.

From the above results, we found that the temporal variations in water surface level/flow depth and flow velocity were different, especially at the peak. In the following sections, we compare the spatial distribution of the maximum values of the physical quantities to identify the areas where the variability is particularly large.

3.2. Characteristics of maximum water surface level and maximum flow velocity and the spatial distribution of their statistics

(Figures 5 to 8) show the spatial distributions of the statistics (mean and standard deviation) for the maximum water surface levels and velocities calculated from each numerical tsunami model. Here, only the grids that were inundated by all the models were extracted, and the statistics were calculated for each grid.

The overall trend of the maximum water surface level in Kochi City indicates that the water surface level decreases as it moves upstream from the coast to the city (Figure 5, upper panel). The tsunami arriving from the offshore area was blocked by the coastal dunes, and the water surface level rose to over 10 m. The tsunami overflows the dunes and inundates behind the lagoonal lowlands. In addition, tsunamis entering Urado Bay run-up to the city along the rivers in the center of the area. The height of the tsunami is approximately 3–5 m in Urado Bay and the rivers and approximately 1–2 m in the city. The standard deviation of the maximum water surface level is distributed in the range of several tens of centimeters in general, but it varies greatly, exceeding 1 m in the area behind the dunes (Figure 5, lower panel). In (Figure 6), the maximum flow velocity is large at the mouth of Urado Bay (about 10 m/s on average) and along the rivers, and the tsunami overflows the river levees and inundates the city. In the land area, large values can be observed on the coastal dunes. The standard deviation of the maximum flow velocity is approximately 2.5 m/s at the mouth of Urado Bay, which is almost the same as that of the mean.

In Susaki City, the average of the highest water surface level was greater than 10 m in all areas, both in the sea and on land (Figure 7). The area has a ria coastline, which means that tsunamis tend to concentrate at the back of the bay, and the water surface level on land is amplified because of the steep, mountainous terrain behind the plains. The highest water surface level at the back of Susaki Bay is lower than that of Nomi Bay and other western bays because of the shielding effect of the breakwater at the mouth of the bay. As for the distribution trend of the maximum flow velocity, large velocities are generated in the sea area (Figure 8). The magnitudes of both the mean and standard deviation are particularly pronounced on the open sea side of the breakwater at the mouth of the bay (near the output point S1).

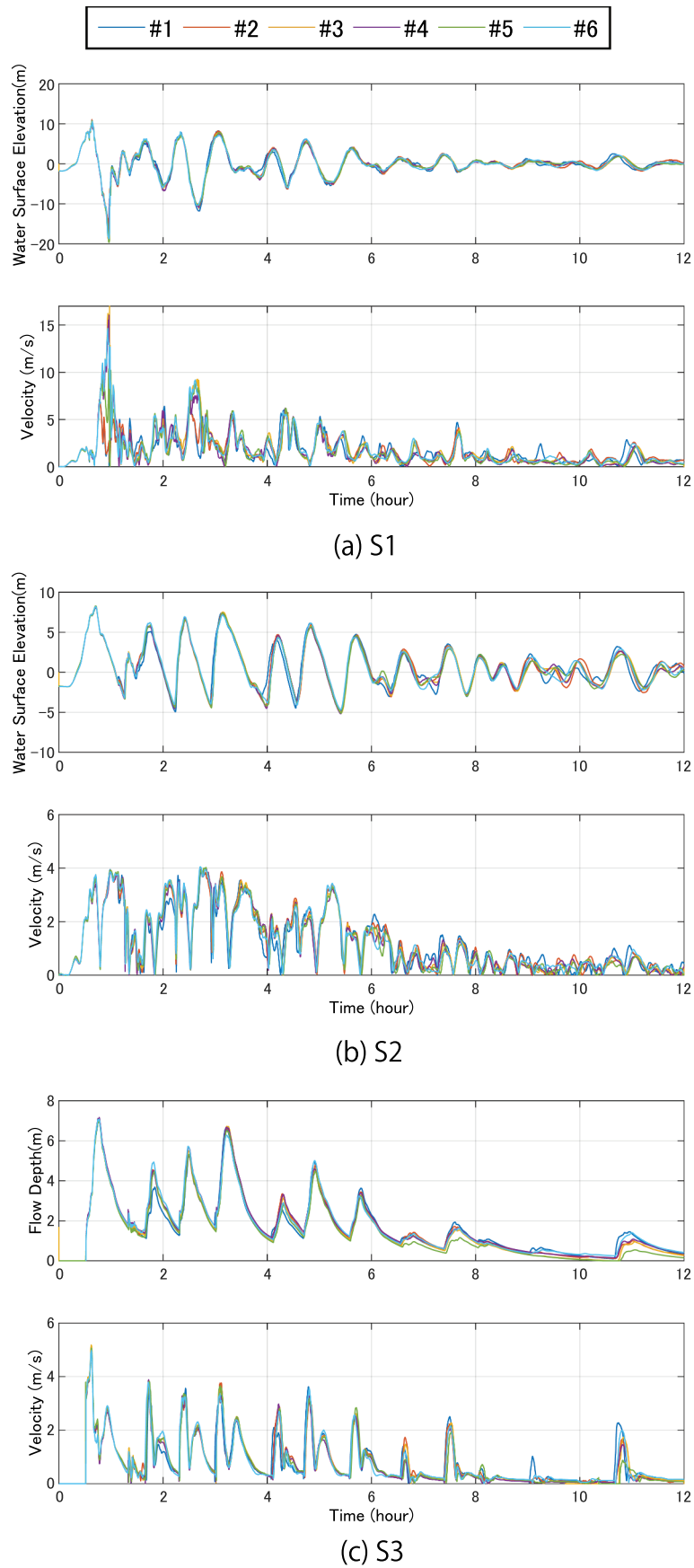


Figure 4. Time series of water surface Elevation, flow depth and flow velocity at the locations shown in Figure 2. The color of the lines in the figures corresponds to the model # in the legend placed on top of the panels.

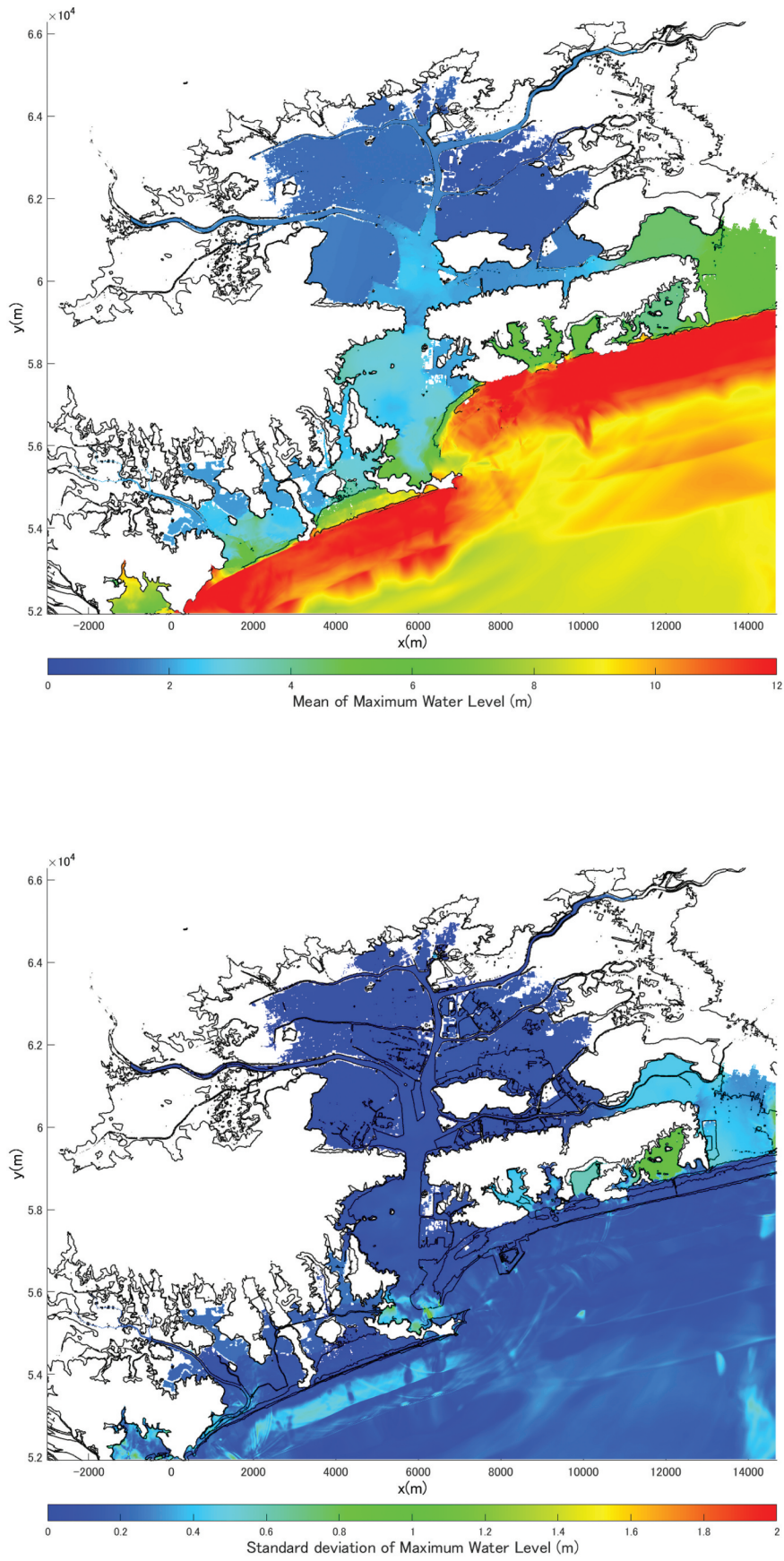


Figure 5. Spatial distribution of statistics for the maximum water surface level in Kochi City. Upper panel: Mean, Lower panel: Standard deviation.

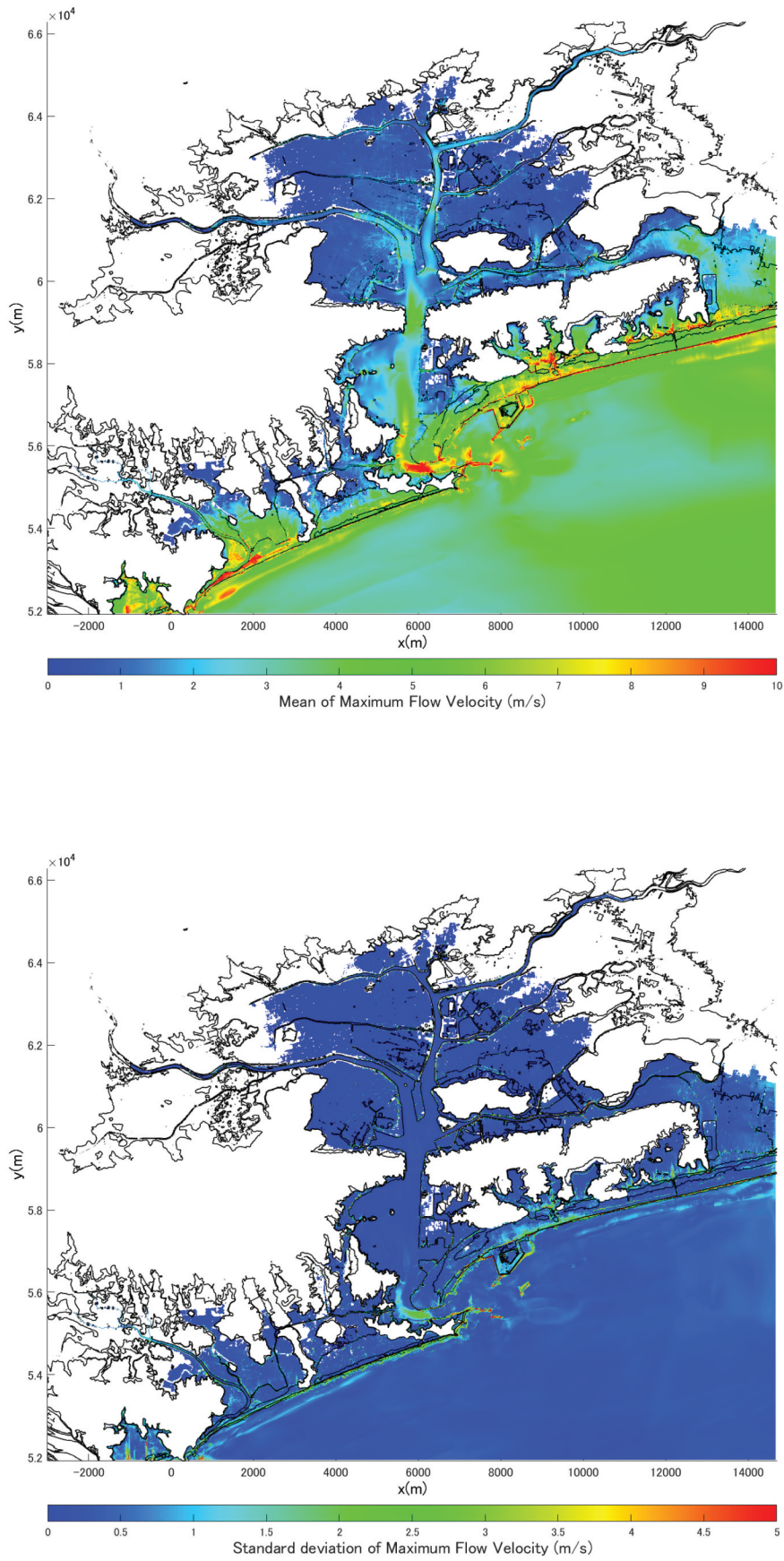


Figure 6. Spatial distribution of statistics for the maximum flow velocity in Kochi City. Upper panel: Mean, Lower panel: Standard deviation.

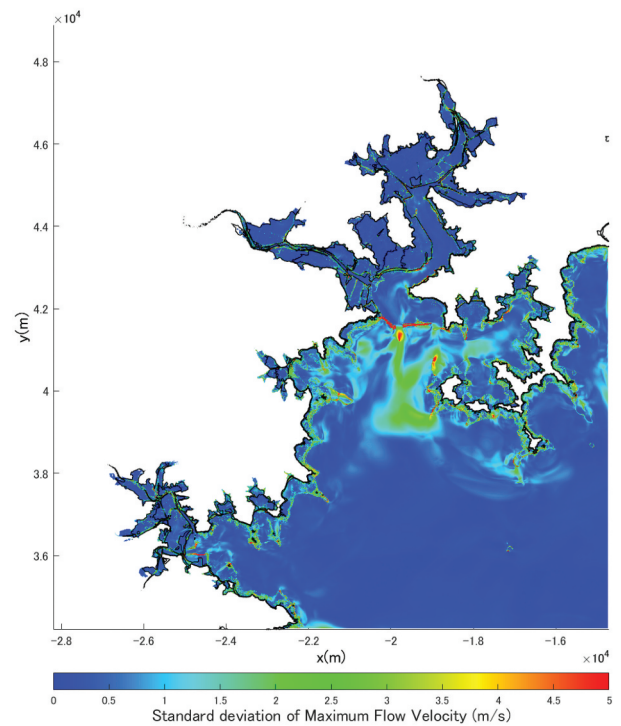
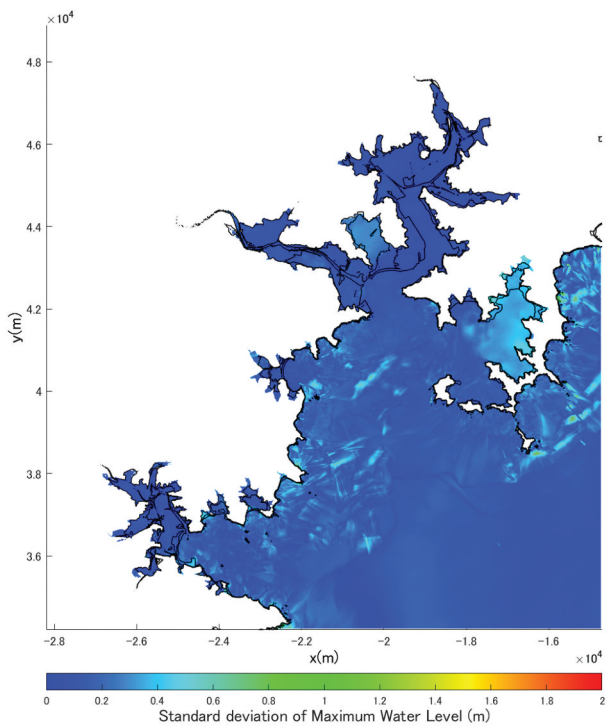
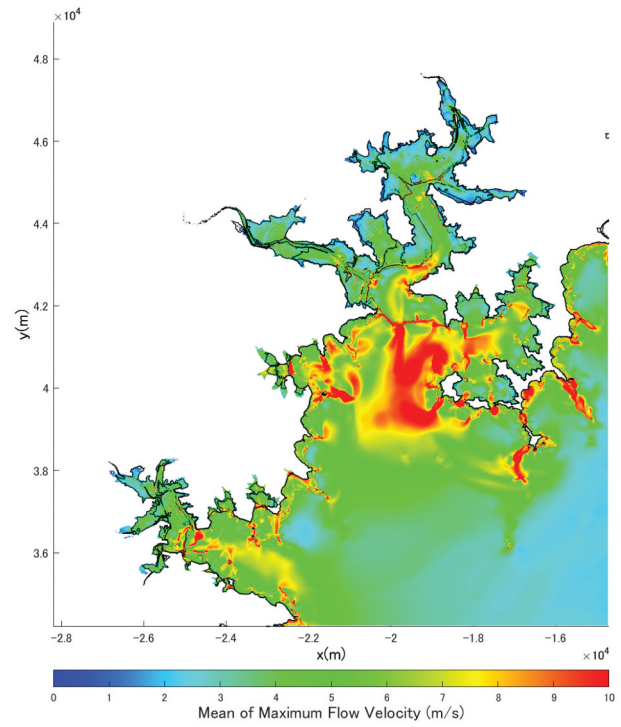
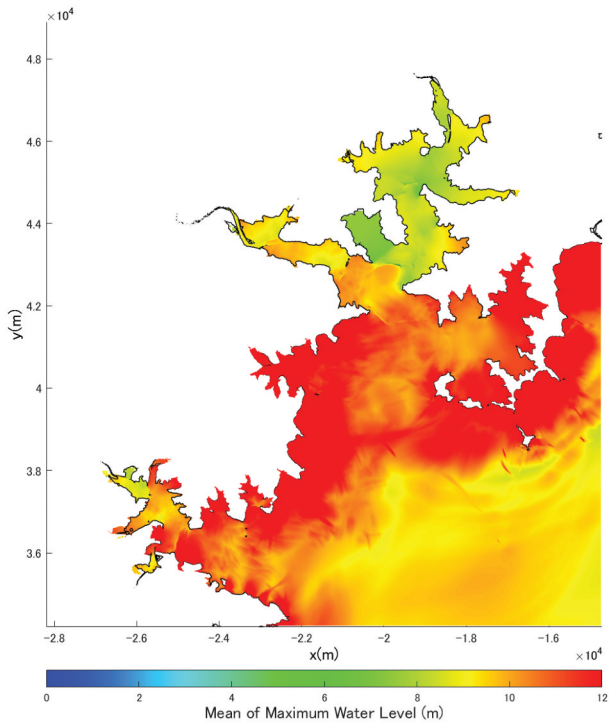


Figure 7. Spatial distribution of statistics for the maximum water surface level in Susaki City. Upper panel: Mean, Lower panel: Standard deviation.

Figure 8. Spatial distribution of statistics for the maximum flow velocity in Susaki City. Upper panel: Mean, Lower panel: Standard deviation.

3.3. Characteristics of maximum flow depth and maximum momentum flux and the spatial distribution of their statistics

Flow depth and momentum flux, which are physical quantities based on the surface of the ground, are used to evaluate in detail the tsunami inundation

situation on land (Figures 9 to 12). The trends for the distributions of flow depth and momentum flux in Kochi City are the same as those for the water surface level and flow velocity. Because the momentum flux is a physical quantity proportional to the square of the flow velocity, it is expected to be large, especially on coastal dunes. The standard deviation of the momentum flux is is

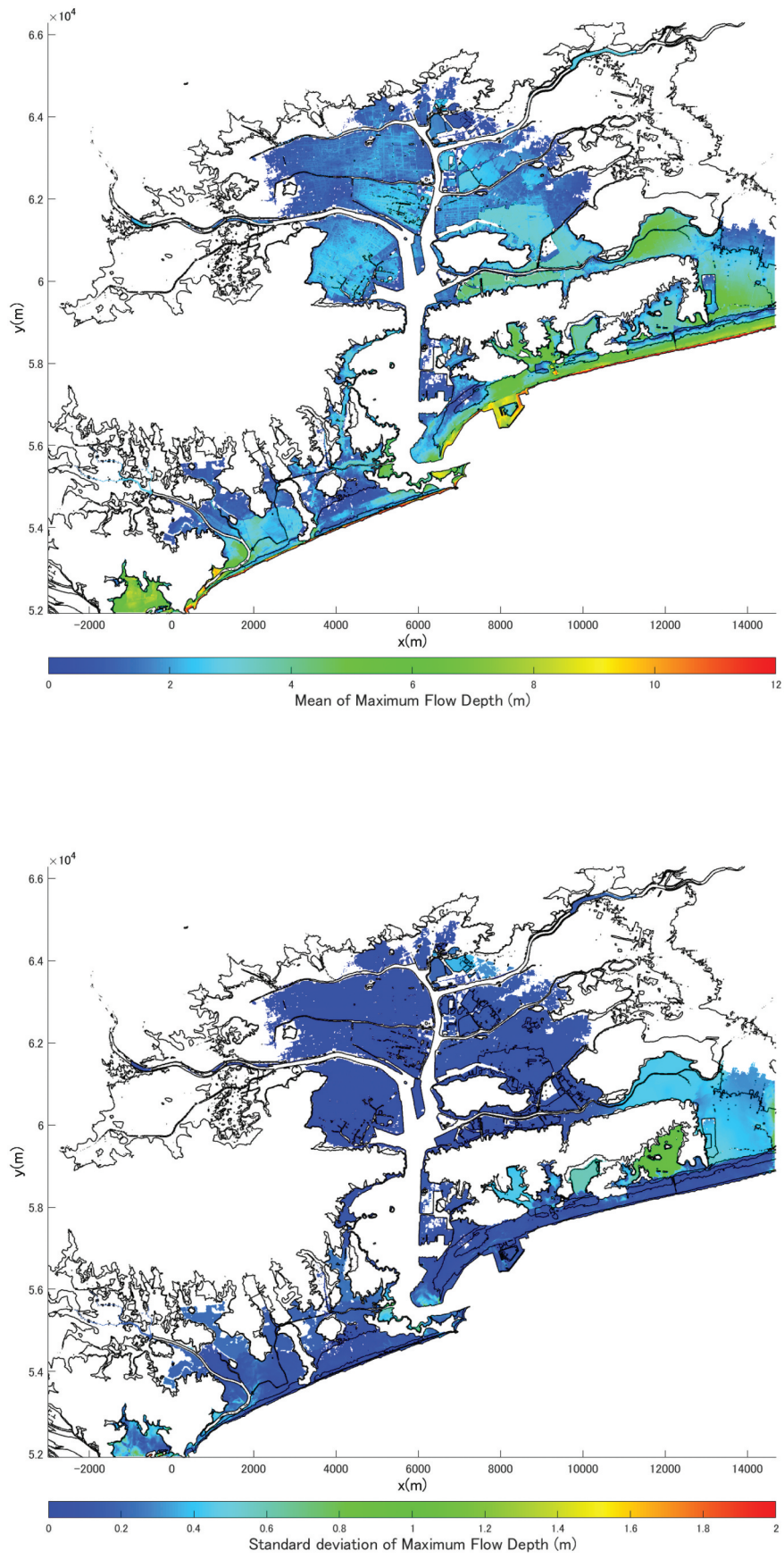


Figure 9. Spatial distribution of statistics for the maximum flow depth in Kochi City. Upper panel: Mean, Lower panel: Standard deviation.

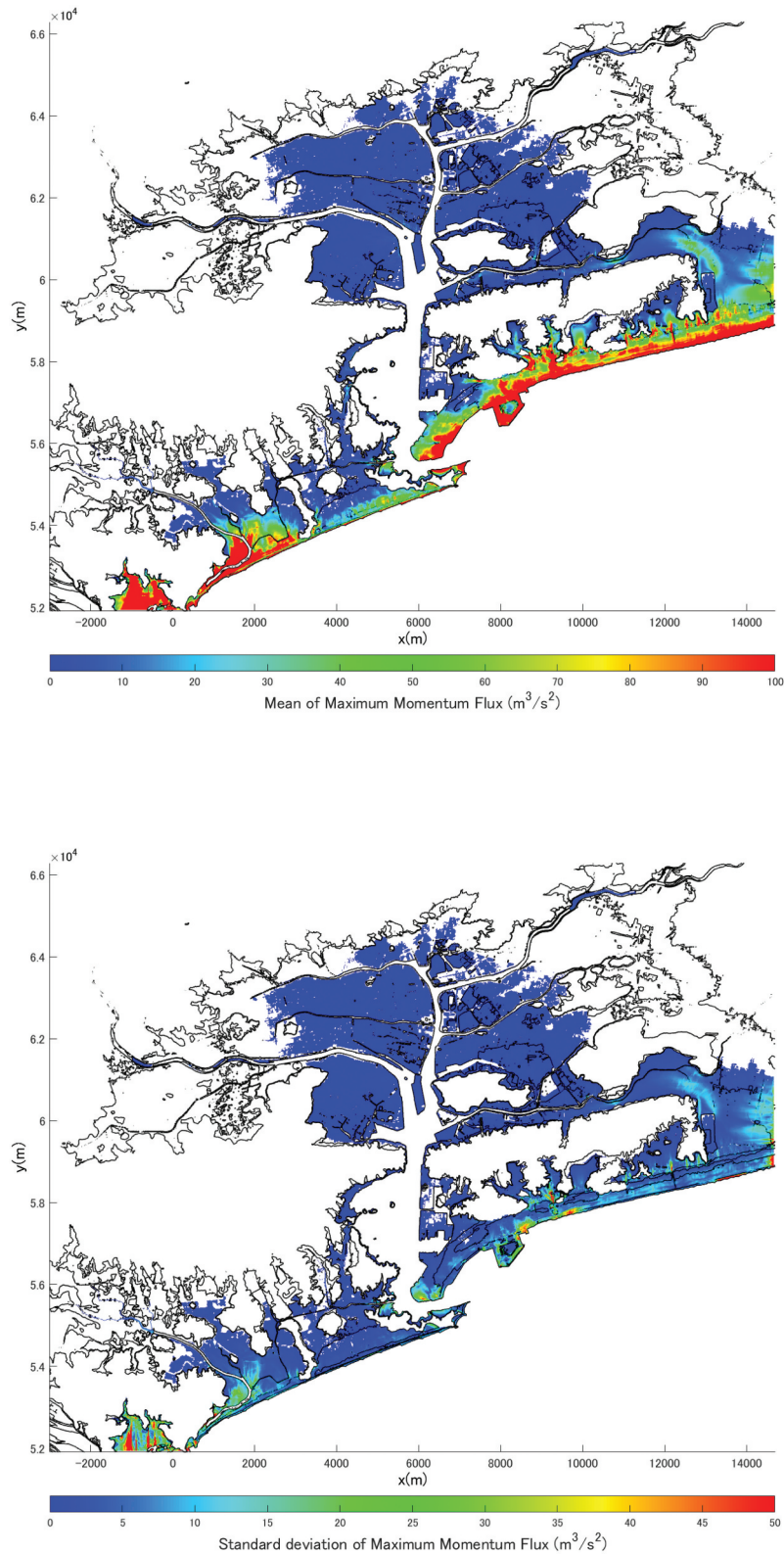


Figure 10. Spatial distribution of statistics for the maximum momentum flux in Kochi City. Upper panel: Mean, Lower panel: Standard deviation.

relatively large near the eastern boundary of the domain. This is due to the difference in the momentum flux coming in from the adjacent 30 m grid domain by the spatial nesting calculation.

Let us now examine the changes in the physical quantities on transects A–A' and B–B' shown in (Figure 2 and Table 4), and analyze the differences

between the coastal areas having large values for standard deviation and the inland urban areas having small values. (Figures 13 and 14). On transect A–A', the tsunami overflows the dune and inundates the area behind it (Figure 13(a)). A large difference in the flow depth was observed between the models (Figure 13(b,c)). The changes in the standard

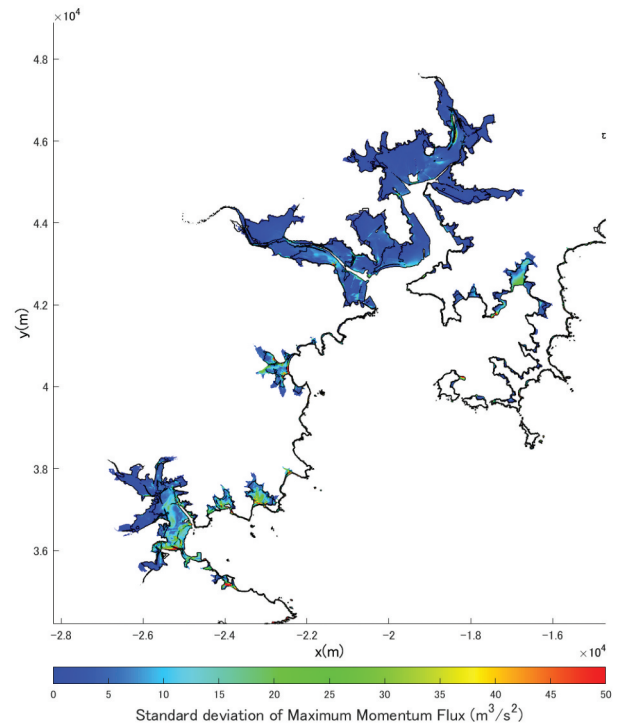
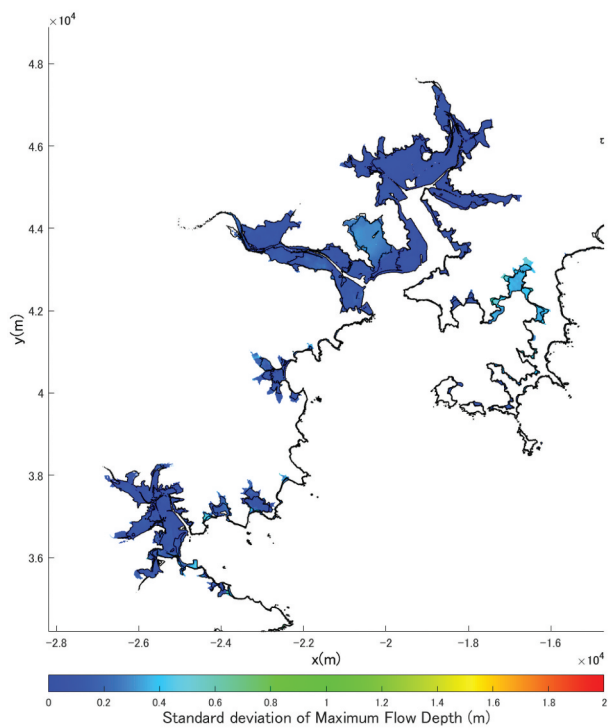
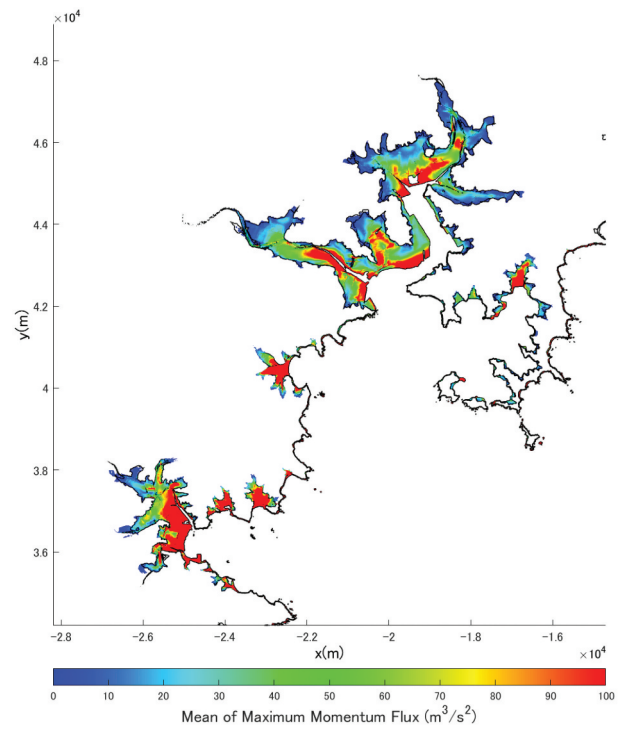
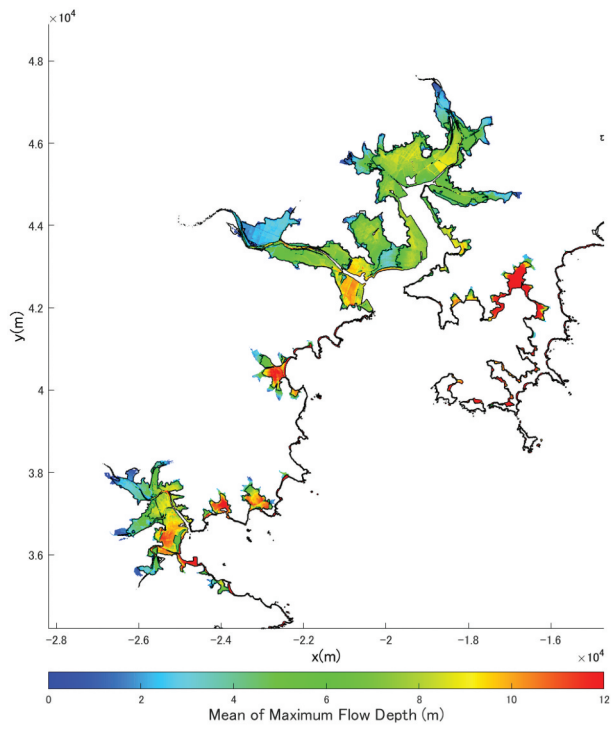


Figure 11. Spatial distribution of statistics for the maximum flow depth in Susaki City. Upper panel: Mean, Lower panel: Standard deviation.

Figure 12. Spatial distribution of statistics for the maximum momentum flux in Susaki City. Top: Mean, Bottom: Standard deviation.

deviation and coefficient of variation (CV) in (Figure 13(d,e)) show that these values peaked at the rear of the dune. In the area behind the dune, the flow depth increased, while the momentum flux tended to decrease. These results suggest that the difference in flow depth and momentum fluxes,

especially when the water overflowed the dune, resulted in a difference in the inflow rate behind the dune and affected the variation in flow depth. For transect B–B', the tsunami overflowed the riverside and inundated the urban area in the area below sea level (Figure 14(a)). The mean and standard deviation

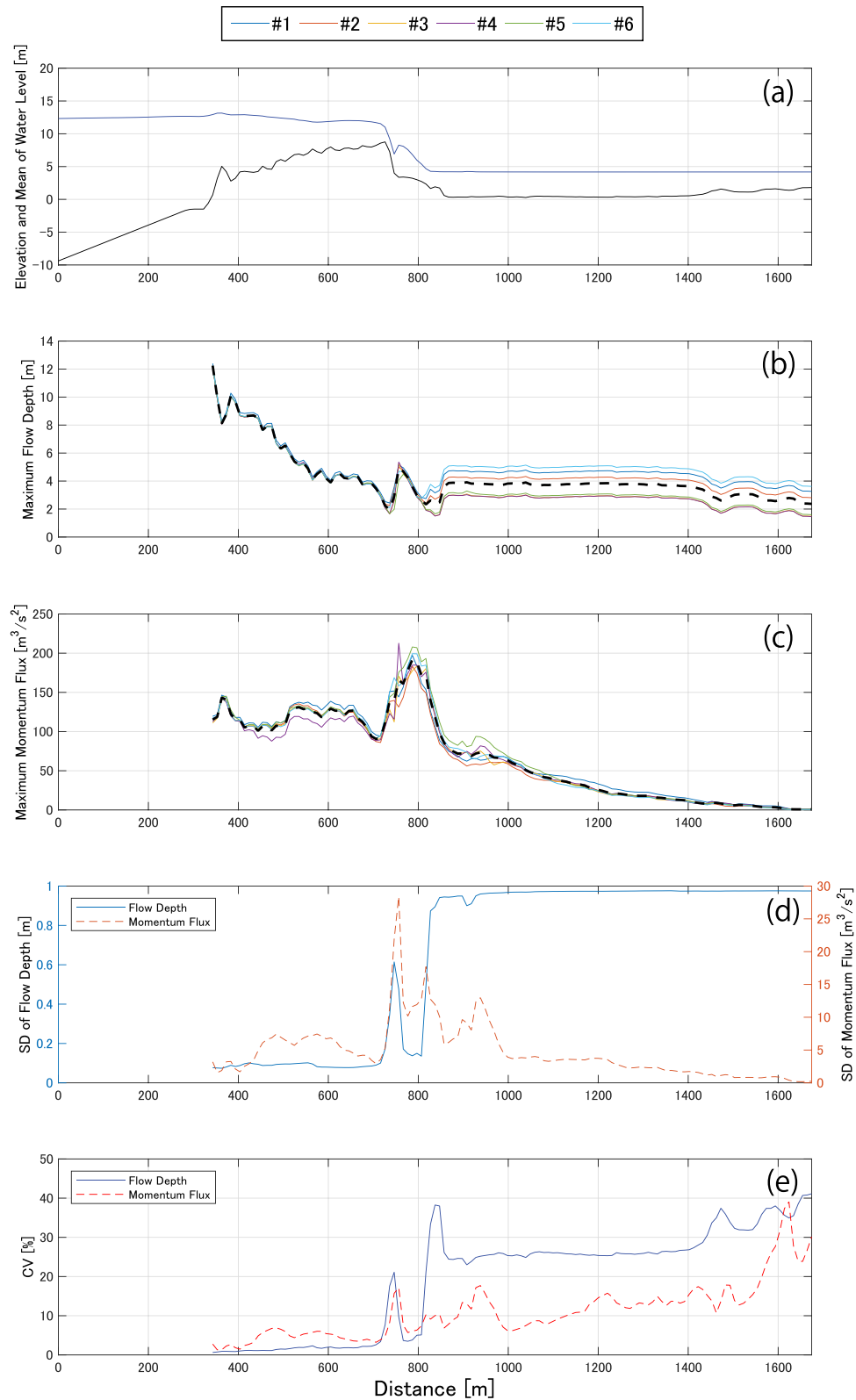


Figure 13. Comparison of the maximum values of tsunami physical quantities on the transect A-A'. Here, (a) is the ground elevation and the water surface level averaged over all models, (b) and (c) the solid line is the overlay of each model for maximum flow depth and momentum flux, the black dotted line is the average of all models, (d) is the standard deviation (SD) of maximum flow depth and maximum momentum flux, and (e) is the coefficient of variation (CV). The colors of the lines in (b) and (c) correspond to the model # in the legend placed on top of the panels.

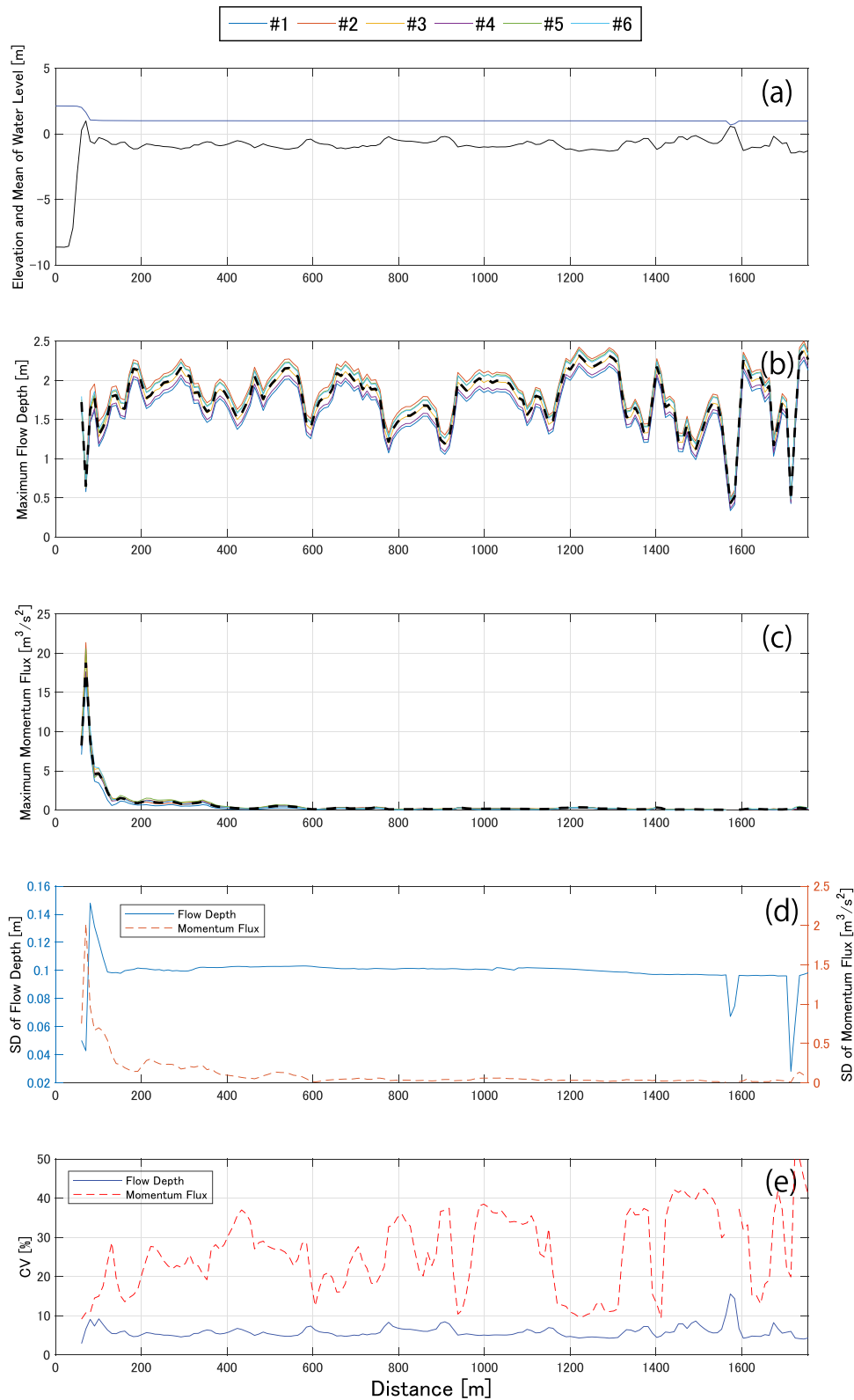


Figure 14. Comparison of the maximum values of tsunami physical quantities on the transect B-B'. The details of (a)-(e) are the same as in Figure 13.

of the flow depths are approximately 2 m and 0.1 m, respectively, although they vary depending on the ground level. The momentum flux is large only in the vicinity of the river and becomes almost zero in the urban area inland from the river. The standard deviations of the fluxes are similar.

Thus, the differences in the urban area (transect B-B') between the models are much smaller than those in the coastal area (transect A-A'). However, as can be seen in (Figure 14(e)), the CV of the momentum flux was calculated to be larger, by approximately 30–40%. This is simply because both the mean and the

standard deviation of the momentum fluxes are small, and thus the CV is apparently large. In Susaki City, most of the land area is inundated, and the mean values of flow depth and momentum flux tend to decrease as the ground elevation increases. In contrast to the back of Nomi Bay (east of Susaki Bay), where the flow depth exceeds 10 m in all areas, the

scale of inundation at the back of Susaki Bay is small. This is due to the energy shielding effect of the breakwater installed at the mouth of the bay, as described above. The standard deviations are distributed according to the magnitude of the mean, and this is also true for the momentum fluxes. As can be seen in (Figure 15(a)), the inundation height of the tsunami is

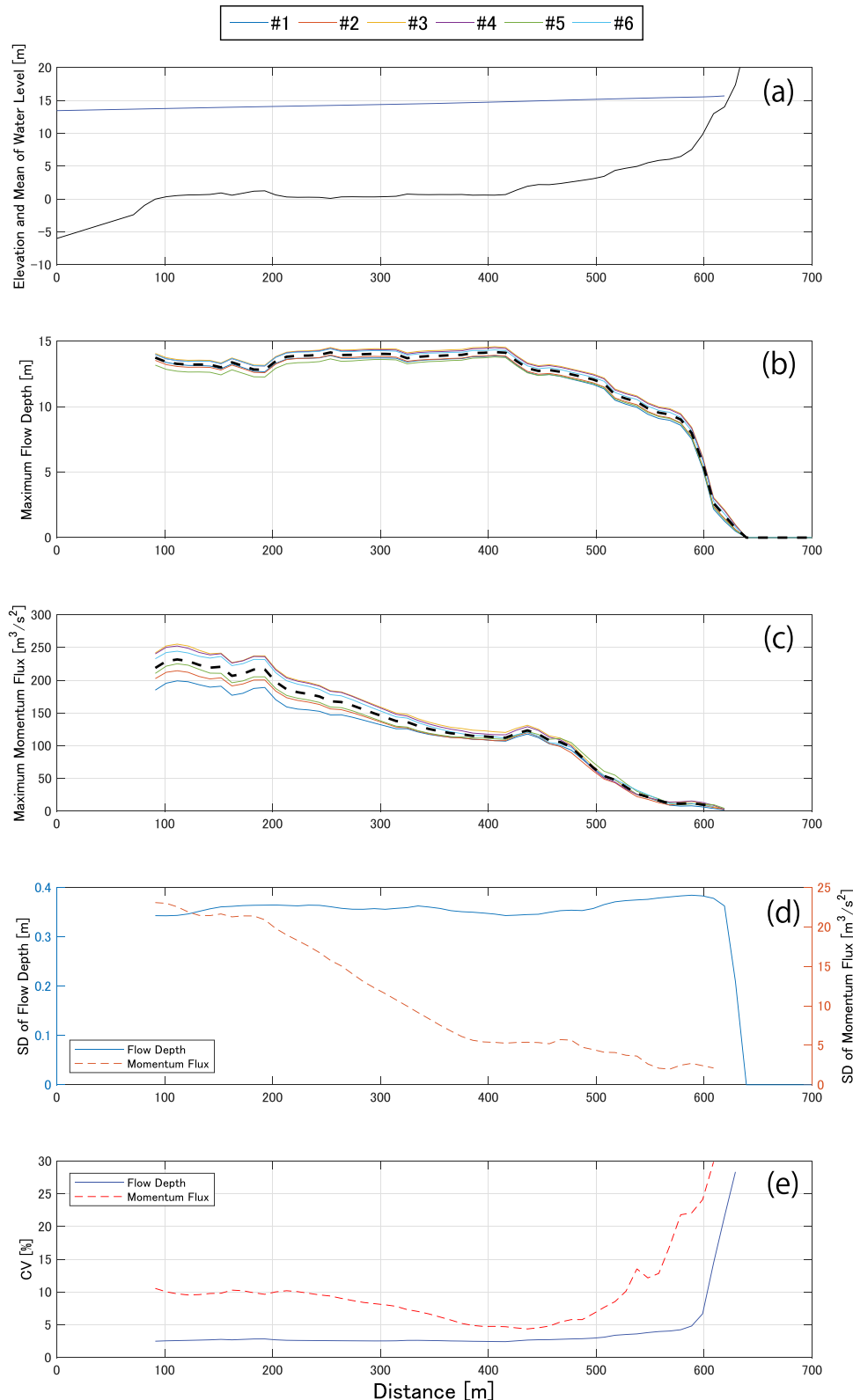


Figure 15. Comparison of the maximum values of tsunami physical quantities on the transect C-C'. The details of (a)-(e) are the same as in Figure 13.

more than 14–15 m from offshore to onshore. The flow depth is almost constant over a distance of 100–400 m, and it decreases sharply near the steep cliffs. The momentum flux gradually decreases from the shoreline. The coefficients of variation up to a distance of approximately 500 m are 2–3% for the flow depth and 5–10% for the momentum flux. We concluded that the variability is smaller than that of the coastal area of Kochi City (transect A–A') (Figure 15(e)).

4. Quantitative evaluation of the overall simulation variability generated by the tsunami inundation model

In Section 3, we clarified the spatio-temporal trend of the variation in physical quantities among tsunami inundation models. The results obtained here can be used as clues to identify the differences in the simulation results and the errors in the models themselves in tsunami hazard assessment. However, users of tsunami inundation models should be aware that there will be some variation in the simulation results locally and should pay attention to the extent to which the simulation results of their model are consistent or different from those of other models in general. This is important for considering the reliability of the results when simulations are conducted for the purpose of tsunami hazard mapping.

Several studies have evaluated the differences between tsunami inundation models. Horrillo et al. (2015) compared the numerical solutions of tsunami inundation models with benchmark problems from hydraulic experiments. They also verified the accuracy of the models based on the existing acceptable error for the water surface level and run-up height. In addition, Montoya et al. (2016) and Lynett et al. (2017) investigated the validity of the models used and the variability in the models by comparing the data observed for the 2011 Tohoku tsunami with the results of several simulations. The studies presented here qualitatively clarify the differences in the temporal or spatial distribution of the physical quantities of the tsunami, especially those presented in the previous section, but do not specifically address the inter-model differences that occur in the entire inundation area.

Against this background, we propose in this section a simple and quantitative method to evaluate the overall variability in tsunami inundation models. Specifically, the total physical quantities, such as inundation area, maximum flow depth, and maximum momentum flux are calculated by area integration, and the statistics (mean and confidence interval) of the models are presented. Moreover, the variability caused by changing the values of various parameters and computational environment adopted in a single model is also clarified.

4.1. Evaluation methods

To calculate the total amount of physical quantities for each tsunami inundation model, the following equation is defined:

$$\iint_S f(x, y) dS \approx \sum_{j=1}^{ny} \sum_{i=1}^{nx} f_{ij} \Delta x \Delta y \quad (4)$$

where $f(x, y)$ is the continuous function of the physical quantity, S is the area, (i, j) , (nx, ny) , and $(\Delta x, \Delta y)$ are the indices for the discrete grid in the horizontal (x, y) direction, the number of grids in the computational domain, and the spatial grid spacing, respectively. In addition, f_{ij} is a discrete function for $f(x, y)$, which can be expressed by the following equation:

$$f_{ij} = \begin{cases} 1, & \text{for } D_{ij} > 0 \\ 0, & \text{for } D_{ij} = 0 \end{cases} \quad (5)$$

$$f_{ij} = D_{ij} \quad (6)$$

$$f_{ij} = (Q^2/D)_{ij} \quad (7)$$

where Q is the discharge rate per unit width. Based on Equation (4), Equations (5), (6), and (7) can be computed as quantities that define the inundation area, the area integral of the maximum flow depth, and the area integral of the maximum momentum flux, respectively.

4.2. Variation of inundation area between tsunami inundation models

From the previous results, it is expected that the inundation area and the run-up limit of the land area will also differ between the models. Considering that this affects the reliability of the tsunami hazard map, we investigated the variation in inundation areas between tsunami inundation models.

(Figure 16) shows graphs of the cumulative change in the inundation area against the maximum flow depth. The horizontal axis is the reciprocal of the flow depth, and the flow depth decreases as the value increases, which corresponds to the situation where the tsunami runs inland from the coast. The minimum flow depth determined as the inundation area was 0.01 m. The mean and standard deviation of the total inundation area are 49 km² and 0.74 km², respectively, in Kochi City (CV: 1.5%), and 13.5 km² and 0.11 km², respectively, in Susaki City (CV: 0.8%). Although there is a difference in the size of the flooded area between the two, owing to the different topographical conditions, the variation in the total flooded area or the flooding limit is negligible. Here, we examined areas where significant differences occurred between the models. In the case of Kochi City, the standard deviation shows an increasing trend from $1/FD = 0.18$, (flow depth:

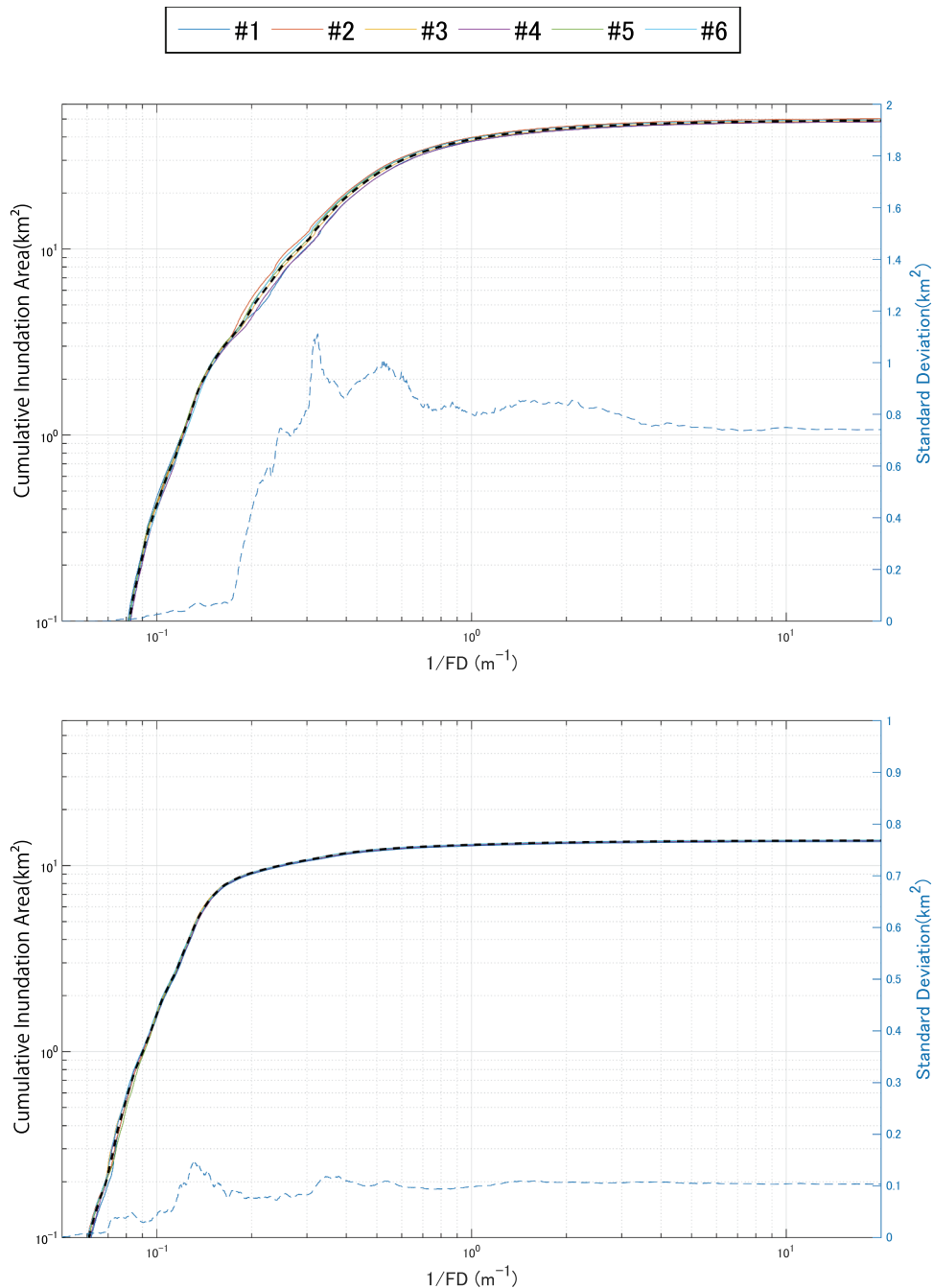


Figure 16. Cumulative and standard deviation change in the inundation area with respect to maximum flow depth. Upper panel: Kochi City, Lower panel: Susaki City. The solid line in the figure shows the results for each model, the black dashed line is the mean for all models, and the blue dashed line is the standard deviation. The colors of the other lines correspond to the model # in the legend placed on top of the panels.

5.5 m), and the line representing each model deviates from the mean line in the graph. Subsequently, the standard deviation is 1.1 km^2 at $1/FD = 0.32$ (flow depth: 3.1 m) and then converges to a constant value (about 0.7 km^2). However, in Susaki City, the standard deviation was 0.14 km^2 at $1/FD = 0.13$ (flow depth: 7.7 m), and no significant difference was observed overall on the graph.

The statistics of the inundation area, based on the Cabinet Office (2012), are presented in (Table 5) when the lower limit of flow depth is set to 5 m (the depth at which the second floor of an ordinary house is

submerged), 2 m (the depth at which a wooden house is completely destroyed or washed away), 1 m (the depth at which the mortality rate is 100% in terms of human casualties due to tsunami), and 0.3 m (the depth at which evacuation becomes difficult). The CV in Susaki City is always less than 1%. The reason why the difference in inundation area was evaluated as small is that almost the entire city is inundated because of the narrow land, which is due to the topographical features of the ria coast. In contrast, the CV in Kochi City, which has low-lying flat areas, has relatively large values. When estimating tsunami damage using

Table 5. Statistics of cumulative inundation area for each flow depth. Left: Kochi City, Right: Susaki City.

	Flow depth					Flow depth			
	5 m	2 m	1 m	0.3 m		5 m	2 m	1 m	0.3 m
Mean [km ²]	4.79	25.3	38.8	46.7	Mean [km ²]	9.12	12.2	12.9	13.4
SD [km ²]	0.42	0.98	0.80	0.78	SD [km ²]	0.08	0.10	0.10	0.11
CV [%]	8.77	3.87	2.06	1.67	CV [%]	0.85	0.85	0.76	0.80

flow depths, it should be assumed that variations will occur because of differences in topographical conditions.

4.3. Variation among tsunami inundation models estimated from total physical quantities

Based on Equations (4), (6), and (7), the area integrals of the maximum flow depth and maximum momentum flux were calculated to evaluate the overall variability among tsunami inundation models. (Figures 17 and 18) compare the values obtained by each model, and (Tables 6 and 7) show the statistics estimated using the t-distribution. The mean values and their 99% confidence intervals (CIs) are shown in the figures and tables, respectively.

From the figures, it is clear that there are differences between the results of each model. In particular, the area integrals calculated for models #1 and #2 are different, even though the values of the parameters used are exactly the same (see Table 3). The reason for this may be due to differences in the handling of nonlinear terms in the source code, as mentioned earlier, but it is difficult to specify further at present. The coefficients of variation from (Tables 6 and 7) are less than 5% in all cases, and even the area integral of the maximum flow depth in Susaki City is as small as 1%. As in the case of the inundation area, Kochi City shows greater variation than Susaki City.

In this study, the parameter settings that the participating research institutes usually employed in tsunami simulations were used. Therefore, the variations obtained reflect the settings that are usually employed in our practical tsunami simulations. Although these values are limited by the type of numerical model used in this study (the finite difference method based on the nonlinear shallow water equations), they may be useful for users to confirm the reliability of the models used in tsunami inundation simulations.

4.4. Variation of tsunami inundation model due to setting parameters and computational environment

Next, we investigate the differences caused by the parameters of the tsunami inundation model and the various conditions of the simulation. A case study was conducted using the topography of Kochi City based on Model #4. The setting conditions for each case are

summarized in (Tables 8 and 9). In Case A, the parameters used in the tsunami inundation model, i.e. the upper limit of flow velocity, censored flow depth, and gravity acceleration, were changed, and in Case B, the computational environment, such as the CPU, compiler, and compiler options, was changed. Then, the area integrals of the maximum flow depth and maximum momentum flux were obtained using the same method as that used in the evaluation in Section 4.3. The results are shown in (Figures 19 and 20), (Tables 10 and 11).

For Case A, the width of the confidence interval and CV were smaller than those obtained in the previous section. Therefore, it is clear that changing the value of any parameter in the source code does not have as much impact as the result obtained in Section 4.3 (the variation between multiple tsunami inundation models). Thus, we examined the parameters that were found to be particularly different from the reference condition (Case 0). For maximum flow depth, changing the minimum flow depth of the bottom friction term (Case A4) results in a larger value than changing the minimum flow depth at the tip of the run-up, which affects the advection term (Case A3). As for the maximum momentum flux, when the upper limit of the flow velocity is changed, Case A1 has a larger area integral value, and Case A2 has a smaller area integral value. However, when the minimum flow depth was changed (Cases A3 and A4), almost no difference was observed. These results indicate that the parameters that affect the simulation results are the minimum flow depth of the bottom friction term for the flow depth and the upper limit of the flow velocity for the momentum flux.

For Case B, the CV was 0.04% for the maximum flow depth and 0.05% for the maximum momentum flux. Therefore, we can conclude that the variation in the results of Model #4 is sufficiently small compared with other conditions owing to the difference in the precision of the real numbers used (single precision or double precision), the computer (CPU), compiler, and compiler options. Incidentally, the single-precision real number calculation yields the same results as the double-precision real number calculation, although the calculation time is significantly reduced.

5. Conclusions

In this study, we simulated a hypothetical tsunami scenario with equivalent input conditions such as topographic data and tsunami source models for several standard tsunami inundation models, and analyzed the

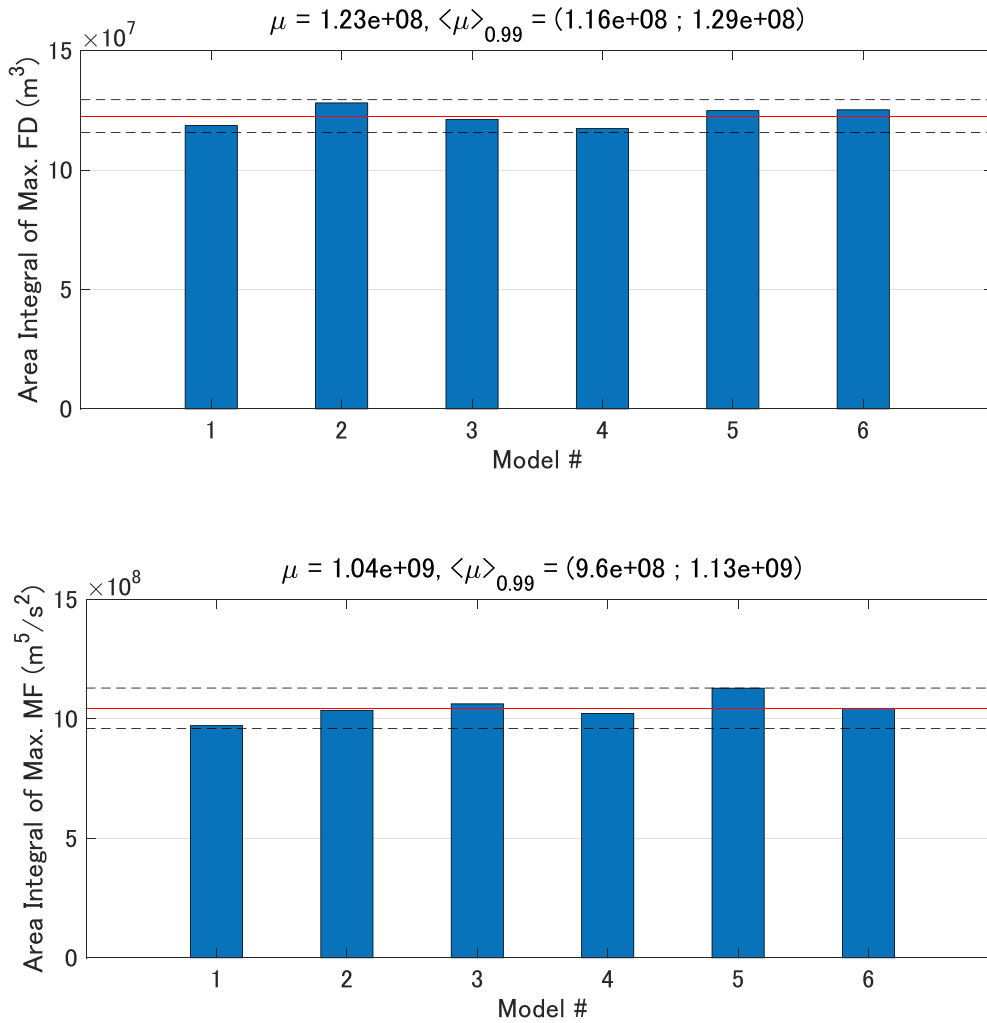


Figure 17. Comparison of the area integral of the maximum flow depth (Max. FD) and maximum momentum flux (Max. MF) calculated from each numerical model in the case of Kochi City. The red solid line shows the mean value μ and the black dashed line shows the 99% confidence interval.

obtained results spatially and temporally. As a result, we were able to clarify the characteristics of the inter-model variability in the physical quantities of tsunamis that propagate and inundate on real topographies, and the magnitude of the variability was quantitatively evaluated. The findings of this study are as follows.

The temporal variations in the water level and flow velocity were generally similar, but the difference was large at the maxima and minima. Therefore, the statistics of the spatial distribution of the maximum geophysical quantities were obtained to investigate the points at which the variation became large. In the ocean, both the mean and standard deviation of the flow velocity tended to be large in areas where the tsunami flow tended to converge, such as rivers and breakwater openings. On land, different characteristics were observed depending on the topographical conditions. In Kochi City, where low-lying areas are scattered, the differences caused by the overflow of sand dunes near the coast appeared as a variation in flow depths in the area directly behind. A tendency for the variability to increase near the spatial connection boundary was also revealed. In Susaki City, the water level was greater than

10 m owing to the effect of tsunami amplification by the ria coast, but the standard deviation was less than several tens of centimeters, and the CV was only a few percent. The variability in the simulation results for Susaki City was smaller than that for Kochi City.

Next, we proposed a method to compare the variability between tsunami inundation models based on the integrated values of various physical quantities and applied the method to this simulation. As for the inundation area, the CV of the total inundation area for both Kochi City and Susaki City was approximately 1%, and the variation around the inundation limit was small. However, Kochi City indicated a large variation in the range of flow depth (2–5 m), which is the standard for evaluating tsunami damage. Statistics were obtained from the area integrals for the maximum flow depth and maximum momentum flux, and the CV was less than 5%. The mean of the area integrals and their 99% CIs were also presented. Similarly, the effects of different setting parameters and computing environments on the simulation results were evaluated for a single model. In both cases, the variability was smaller than that of multiple tsunami inundation models. In terms of

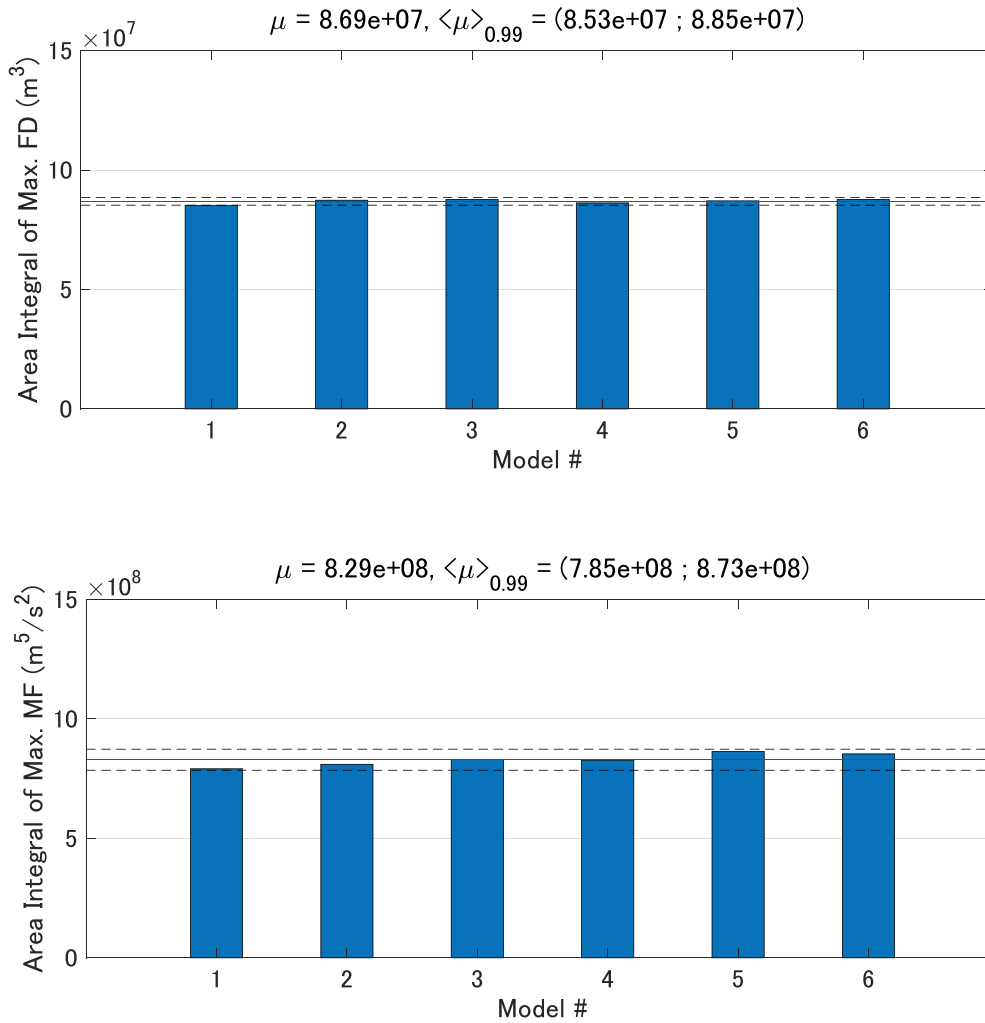


Figure 18. Comparison of the area integral of the maximum flow depth (Max. FD) and maximum momentum flux (Max. MF) calculated from each numerical model in the case of Susaki City. The red solid line shows the mean value μ and the black dashed line shows the 99% confidence interval.

Table 6. Statistical estimation results of the area integral of the maximum flow depth (MFD) and the maximum momentum flux (MMF) for multiple tsunami inundation models in the case of Kochi City.

	Mean	99% CI of the mean		Standard deviation	CV [%]
		lower limit	higher limit		
Area Integral of MFD [m ³]	1.23×10^8	1.16×10^8	1.29×10^8	4.19×10^6	3.42
Area Integral of MMF [m ⁵ /s ²]	1.04×10^9	9.60×10^8	1.13×10^9	5.15×10^7	4.93

Table 7. Statistical estimation results of the area integral of the maximum flow depth (MFD) and the maximum momentum flux (MMF) for multiple tsunami inundation models in the case of Susaki City.

	Mean	99% CI of the mean		Standard deviation	CV [%]
		lower limit	higher limit		
Area Integral of MFD [m ³]	8.69×10^7	8.53×10^7	8.85×10^7	9.96×10^5	1.11
Area Integral of MMF [m ⁵ /s ²]	8.29×10^8	7.85×10^8	8.73×10^8	2.68×10^7	3.23

the different parameter settings, the most influential parameters were the minimum flow depth of the bottom friction term for the flow depth and the upper limit of the flow velocity for the momentum flux. Changes in the computing environment, such as the CPU and compiler, had little effect on the simulation results.

The results presented herein are vital for understanding the reliability of tsunami inundation models during tsunami damage estimation. In other words, even if the same governing equations are used and

tsunami simulations are performed under the same set of parameters (i.e. the parameters used by each research institute in their daily practice), there is a certain degree of variability in the results. This study quantitatively demonstrates, for the first time, the empirical findings of tsunami researchers and engineers. This can serve as useful information to bridge the gap in the awareness of the adequacy of tsunami simulations, particularly in the development of tsunami disaster prevention plans. In general, companies

Table 8. Summary of parameter settings for the case study (Case A) based on Model 4^a.

Case #	Limit of maximum flow velocity [m/s]	Minimum flow depth for dry-wet condition [m]	Minimum flow depth for bottom friction terms [m]	Gravity acceleration [m/s ²]
0	20	1.0E-05	1.0E-02	9.80665
A1	50	1.0E-05	1.0E-02	9.80665
A2	×	1.0E-05	1.0E-02	9.80665
A3	20	1.0E-07	1.0E-02	9.80665
A4	20	1.0E-05	1.0E-05	9.80665
A5	20	1.0E-05	1.0E-02	9.8

^aCase 0 has the same settings as Model 4 shown in Table 3.

Table 9. Summary of parameter settings for the case study (Case B) based on Model 4^a.

Case #	Numeric precision	CPU	Compiler	Option	Computing time [hours]
0	Double	Intel Xeon E5-2667 v3 ^b	Intel Fortran Linux 13.1	ifort -fast -parallel -openmp ^d	16.1
B1	Single	Intel Xeon E5-2667 v3 ^b	Intel Fortran Linux 13.1	ifort -fast -parallel -openmp ^d	9.9
B2	Double	Intel Xeon E5-2667 v3 ^b	Intel Fortran Linux 13.1	ifort -O2	40.6
B3	Double	Intel Xeon E5-2667 v3 ^b	gcc 4.4.7	gfortran -O2 -fopenmp ^d	20.5
B4	Double	Intel Core i7-8700 ^c	gcc 9.2.0	gfortran -O2 -fopenmp ^d	17.9
B5	Double	Intel Core i7-8700 ^c	NAG Fortran Compiler 6.0	nagfor -O2 -openmp ^d	20.8

^aCase 0 has the same settings as Model 4 shown in Table 3.

^b3.20 GHz 20MB Cache 8Cores

^c3.20 GHz 12MB Cache 6Cores

^dEight threads used for the parallelization.

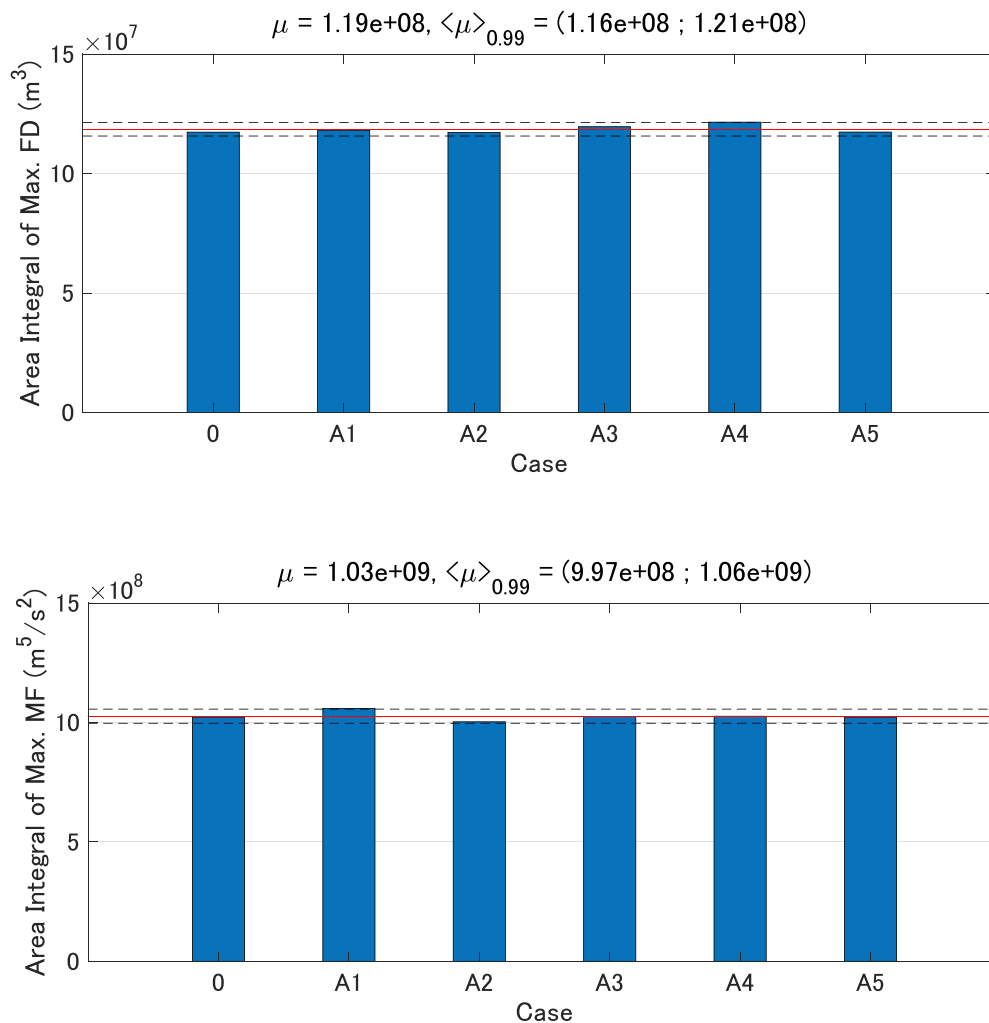


Figure 19. Comparison of the area integral of the maximum flow depth (Max. FD) and maximum momentum flux (Max. MF) for Case A with different calculation conditions based on Model 4. in the case of Kochi City. The red solid line shows the mean value μ and the black dashed line shows the 99% confidence interval.

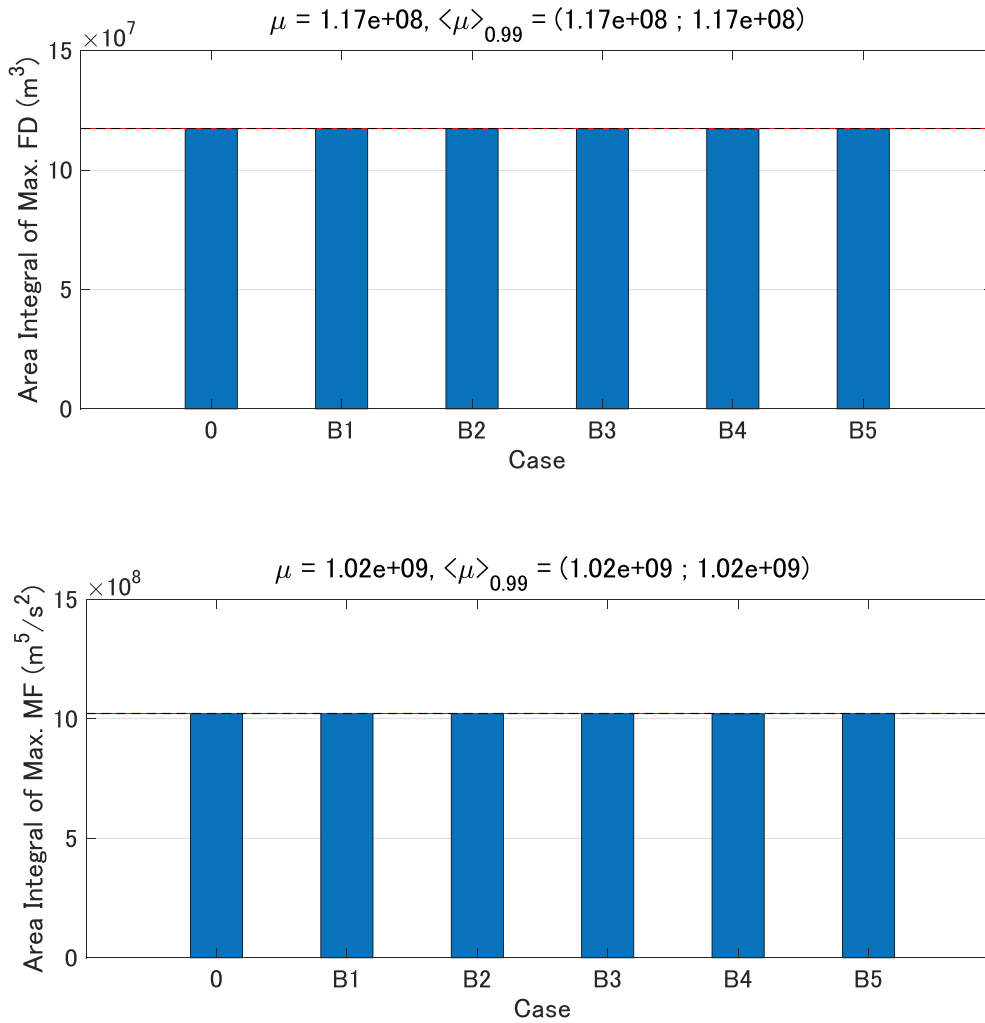


Figure 20. Comparison of the area integral of the maximum flow depth (Max. FD) and maximum momentum flux (Max. MF) for Case B with different calculation conditions based on Model 4. in the case of Kochi City. The red solid line shows the mean value μ and the black dashed line shows the 99% confidence interval.

(clients) ask consultant companies to conduct tsunami simulations individually. Clients require the simulation results to be consistent with the hazard maps

published by the government (in Japan, the Cabinet Office). The findings obtained in this study are expected to help clients recognize that there are insurmountable differences in tsunami simulations, and consequently, promote the smooth progress of tsunami disaster prevention planning research.

Table 10. Statistical estimation results of the area integral of the maximum flow depth (MFD) and the maximum momentum flux (MMF) for Case A.

	Mean	99% CI of the mean		Standard deviation	CV [%]
		lower limit	higher limit		
Area Integral of MFD [m ³]	1.19×10^8	1.16×10^8	1.21×10^8	1.71×10^6	1.45
Area Integral of MMF [m ⁵ /s ²]	1.03×10^9	9.97×10^8	1.06×10^9	1.80×10^7	1.75

The newly proposed method of comparing models using the integrated values of physical quantities can be used not only to evaluate the model reliability, but also to understand the variability and uncertainty of the model parameters. The conditions set in this study are based on a hypothetical event, which is officially published by the Japanese Cabinet Office and widely used by all parties in Japan, so that users of tsunami inundation models can easily perform similar calculations. In

Table 11. Statistical estimation results of the area integral of the maximum flow depth (MFD) and the maximum momentum flux (MMF) for Case B.

	Mean	99% CI of the mean		Standard deviation	CV[%]
		lower limit	higher limit		
Area Integral of MFD [m ³]	1.1736×10^8	1.1729×10^8	1.1735×10^8	4.52×10^4	0.04
Area Integral of MMF [m ⁵ /s ²]	1.0226×10^9	1.0218×10^9	1.0235×10^9	5.09×10^5	0.05

this manner, for example, the statistics on inundation area, maximum inundation depth, and maximum momentum flux obtained in this study can be compared as criteria for users to verify the validity of the models they use. The statistics on the configuration parameters can help users detect errors in their own source codes and improve their models. In addition, the various values of CV and standard deviation presented in this paper may be employed as parameters in the future when considering the uncertainty due to the numerical model itself in PTHA.

However, care should be taken in handling the values given in the paper. In this study, the tsunami scenario of the largest class (M9) was used because it was intended for practical use. On the contrary, in the case of a relatively small tsunami scenario, the parameters near the tip of the tsunami run-up are expected to have a large impact on the results, which may be evaluated as a larger variability than the present results. In addition, only six organizations participated in this project, and the sample size was insufficient for drawing statistical conclusions. To adopt the values obtained by the method proposed in this paper as more reliable reference values, the data should be further updated by examining tsunami scenarios that are not as extremely large in scale as that described above and by increasing the number of models. In the future, it will also be desirable to construct and provide a system that enables users to easily execute the evaluation method proposed in this paper.

Additionally, it is important to compare the effects of different situations in which disaster prevention facilities such as seawalls are taken into account, and different bottom friction laws, to show more realistic and reliable variations in inundation simulation results. Nonlinear dispersive wave models (Boussinesq models) and three-dimensional models (NS models), which are higher-order approximations than conventional shallow water theoretical models, may be applied in practice, and information on these differences should be updated accordingly. It is also important to compare the effects of different situations in which disaster prevention facilities such as seawalls are taken into account and different bottom friction laws to show more realistic and reliable variations in inundation simulation results. Nonlinear dispersive wave models (Boussinesq model) and three-dimensional models (NS model), which are higher-order approximations than conventional shallow water theoretical models, may be applied in practice, and information on these differences should be updated accordingly.

Acknowledgments

This study was conducted as a part of the activities of “a subcommittee for the research review of tsunami effects and its uses (the Coastal Engineering Committee of the Japan Society of Civil Engineering) WG2: Generation, Propagation

and Run-up.” We gratefully acknowledge many advices from the members of this working group.

Disclosure statement

No potential conflict of interest was reported by the author(s).

ORCID

Yoshinori Shigihara  <http://orcid.org/0000-0001-7567-6214>

Kentarō Imai  <http://orcid.org/0000-0002-6611-2625>

Naotaka Yamamoto Chikasada  <http://orcid.org/0000-0003-0332-1929>

Taro Arikawa  <http://orcid.org/0000-0002-7115-2760>

References

- Association for Promotion of Infrastructure Geospatial Information Distribution (AIGID). 2016. “G-spatial Information Center” Accessed 31 March 2021. https://www.geospatial.jp/gp_front in Japanese.
- Baba, T., S. Allgeyer, J. Hossen, P.R. Cummins, H. Tsushima, K. Imai, K. Yamashita, and T. Kato. 2017. “Accurate Numerical Simulation of the Far-field Tsunami Caused by the 2011 Tohoku Earthquake, Including the Effects of Boussinesq Dispersion, Seawater Density Stratification, Elastic Loading, and Gravitational Potential Change.” *Ocean Modeling* 111: 46–54. doi:10.1016/j.ocemod.2017.01.002.
- Baba, T., K. Ando, D. Matsuoka, M. Hyodo, T. Hori, N. Takahashi, R. Obayashi, et al. 2016. “Large-scale, High-speed Tsunami Prediction for the Great Nankai Trough Earthquake on the K Computer.” *Pure and Applied Geophysics* 30:71–84. doi:10.1177/1094342015584090.
- Baba, T., N. Takahashi, Y. Kaneda, K. Ando, D. Matsuoka, and T. Kato. 2015. “Parallel Implementation of Dispersive Tsunami Wave Modeling with a Nesting Algorithm for the 2011 Tohoku Tsunami.” *Pure and Applied Geophysics* 172 (12): 3455–3472. doi:10.1007/s00024-015-1049-2.
- Baba, T., N. Takahashi, Y. Kaneda, Y. Inazawa, and M. Kikkojin. 2014. “Tsunami Inundation Modeling of the 2011 Tohoku Earthquake Using Three-Dimensional Building Data for Sendai, Miyagi Prefecture, Japan.” *Tsunami Events and Lessons Learned, Advances in Natural and Technological Hazards Research* 35: 89–98. doi:10.1007/978-94-007-7269-4_3.
- Cabinet Office, Government of Japan. 2012. “Massive Earthquake Model Review Meeting of the Nankai Trough” Accessed 31 March 2021. <http://www.bousai.go.jp/jishin/nankai/model/index.html> in Japanese
- Fukutani, Y., S. Moriguchi, K. Terada, and Y. Otake. 2021. “Time-Dependent Probabilistic Tsunami Inundation Assessment Using Mode Decomposition to Assess Uncertainty for an Earthquake Scenario.” *Journal of Geophysical Research: Oceans* 126 (7): e2021JC017250. doi:10.1029/2021JC017250.
- George, D. L. 2008. “Augmented Riemann Solvers for the Shallow Water Equations over Variable Topography with Steady States and Inundation.” *Journal of Computational Physics* 227 (6): 3089–3113. doi:10.1016/j.jcp.2007.10.027.

- George, D. L., and R. J. LeVeque. 2006. "Finite Volume Methods and Adaptive Refinement for Global Tsunami Propagation and Local Inundation." *Science of Tsunami Hazards* 24: 319–328.
- Goto, C., and Y. Ogawa. 1997. "IUGG/IOC TIME PROJECT: Numerical Method of Tsunami Simulation with the Leap-frog Scheme, Part-1 Shallow Water Theory and Its Difference Scheme." *Intergovernmental Oceanographic Commission, Manuals and Guides* 35: 43.
- Hayashi, S., and S. Koshimura. 2013. "The 2011 Tohoku Tsunami Flow Velocity Estimation by the Aerial Video Analysis and Numerical Modeling." *Journal of Disaster Research* 8 (4): 561–572. doi:10.20965/jdr.2013.p0561.
- Hoffman, F. O., and J. S. Hammonds. 1994. "Propagation of Uncertainty in Risk Assessments: The Need to Distinguish between Uncertainty Due to Lack of Knowledge and Uncertainty Due to Variability." *Risk Analysis* 14 (5): 707–712. doi:10.1111/j.1539-6924.1994.tb00281.x.
- Horrillo, J., S. T. Grilli, D. Nicolsky, V. Roeber, and J. Zhang. 2015. "Performance Benchmarking Tsunami Models for NTHMP's Inundation Mapping Activities." *Pure and Applied Geophysics* 172 (3–4): 869–884. doi:10.1007/s00024-014-0891-y.
- Imamura, F. 1995. "Tsunami Numerical Simulation with the Staggered Leap-Frog Scheme, Manuscript for TUNAMI Code." School Civil Eng., Asian Insti. Tech. 45.
- Imamura, F. 1996. "Review of Tsunami Simulation with a Finite Difference Method." In *Long-wave Run-up Models*, edited by H. Yeh, P. Liu, and C. Synolakis, 25–42. World Scientific. Singapore: World Scientific.
- Imamura, F. 2009. "Tsunami Modeling: Calculating Inundation and Hazard Maps." In *The Sea Vol.15, Tsunamis*, edited by E. N. Bernard, and A. R. Robinson, 321–332. Cambridge, MA: Harvard University Press.
- Imamura, F., A. C. Yalciner, and G. Ozyurt. 2006. "Tsunami Modelling Manual (TUNAMI Model)" Accessed 31 March 2021. <http://www.tsunami.civil.tohoku.ac.jp/hokusai3/E/projects/manual-ver-3.1.pdf>
- Iwasaki, T., and A. Mano. 1979. "Two-Dimensional Numerical Simulation of Tsunami Run-ups in the Eulerian Description." Proceedings of 26 th the Japanese Conference on Coastal Engineering, JSCE, 70–74. In Japanese.
- Iwase, H., and F. Imamura. 2004. "A New Tsunami Numerical Simulation with Boussinesq-Type Equations Applied for the 1983 Nihonkai-Chubu Earthquake Tsunami." Proceeding of 2nd International Conference on Asia and Pacific Coasts 2003, Chiba, Japan, 1–13.
- Kotani, M., F. Imamura, and N. Shuto. 1998. "New Method of Tsunami Run-up and Estimation of Damage Using GIS Data." *Proceedings of Coastal Engineering in Japan, JSCE* 45: 356–360. in Japanese.
- Kowalik, Z., W. Knight, T. Logan, and P. Whitmore. 2005. "Numerical Modeling of the Global Tsunami: Indonesian Tsunami of 26 December 2004." *Science of Tsunami Hazards* 23 (1): 40–56.
- Kowalik, Z., and T. S. Murty. 1993. *Numerical Modeling of Ocean Dynamics*, 481. Singapore: World Scientific.
- Lynett, P. J., K. Gately, R. Wilson, L. Montoya, D. Arcas, B. Aytore, Y. Bai, et al. 2017. "Inter-model Analysis of Tsunami-induced Coastal Currents." *Ocean Modelling* 114:14–32. doi:10.1016/j.ocemod.2017.04.003.
- Miyoshi, T., W. Suzuki, N. Chikasada, S. Aoi, and S. Akagi. 2019. "Development of Tsunami Simulator TNS." *Technical Note of the National Research Institute for Earth Science and Disaster Resilience* 427. in Japanese.
- Montoya, L., P. Lynett, H. K. Thio, and W. Li. 2016. "Spatial Statistics of Tsunami Overland Flow Properties." *Journal of Waterway, Port, Coastal and Ocean Engineering* 143 (2): 1–8. doi:10.1061/(ASCE)WW.1943-5460.0000363.
- Nicolsky, D., E. Suleimani, and R. Hansen. 2011. "Validation and Verification of a Numerical Model for Tsunami Propagation and Runup." *Pure and Applied Geophysics* 168 (6–7): 1199–1222. doi:10.1007/s00024-010-0231-9.
- Oishi, Y., F. Imamura, and D. Sugawara. 2015. "Near-field Tsunami Inundation Forecast Using the Parallel TUNAMI-N2 Model: Application to the 2011 Tohoku-Oki Earthquake Combined with Source Inversions." *Geophysical Research Letters* 42 (4): 1083–1091. doi:10.1061/(ASCE)WW.1943-5460.0000363.
- Seacoast Office, Water and Disaster Management Bureau and Coast Division, River Department, National Institute for Land and Infrastructure Management, Ministry of Land, Infrastructure, Transport and Tourism (MLIT). 2012. "Guide to Determining the Potential Tsunami Inundation. Ver. 2.00" Accessed 31 March 2021. <http://www.nilim.go.jp/english/disaster/tsunami.pdf>
- Shi, F., J. T. Kirby, J. C. Harris, J. D. Geiman, and S. T. Grilli. 2012. "A High-order Adaptive Time-stepping TVD Solver for Boussinesq Modeling of Breaking Waves and Coastal Inundation." *Ocean Modeling* 43-44: 36–51. doi:10.1016/j.ocemod.2011.12.004.
- Shigihara, Y., and K. Fujima. 2006. "Wave Dispersion Effect in the Indian Ocean Tsunami." *Journal of Disaster Research* 1 (1): 142–147. doi:10.20965/jdr.2006.p0142.
- Shigihara, Y., and K. Fujima. 2014. "An Adequate Dispersive Wave Scheme for Tsunami Simulation." *Coastal Engineering Journal* 56 (1): 1450003. doi:10.1142/S057856341450003X.
- Shuto, N., C. Goto, and F. Imamura. 1990. "Numerical Simulation as a Means of Warning for Near-Field Tsunamis." *Coastal Engineering in Japan* 33 (2): 173–193. doi:10.1080/05785634.1990.11924532.
- Subcommittee for the Research Review of Tsunami Effects and its Uses, Coastal Engineering Committee, Japan Society of Civil Engineers (JSCE) and National Research Institute for Earth Science and Disaster Resilience (NIED). 2018. "The Tsunami Mitigation Research Portal Site." Accessed 31 March 2021. <https://tsunami-portal.bosai.go.jp/en/index>
- Takabatake, T., J. Stolle, K. Hiraishi, N. Kihara, K. Nojima, Y. Shigihara, T. Arikawa, and I. Nistor. 2021. "Inter-Model Comparison for Tsunami Debris Simulation." *Journal of Disaster Research* 17 (7): 1030–1044. In press. doi:10.20965/jdr.2021.p1030.
- Takahashi, T. 1996. "Benchmark Problem 4 the 1993 Okushiri Tsunami - Data, Conditions and Phenomena." In *Long-wave Run-up Models*, edited by H. Yeh, P. Liu and C. Synolakis, 384–403. Singapore: World Scientific.
- Titov, V. V. 2009. "Tsunami Forecasting." In *The Sea Vol.15, Tsunamis*, edited by E. N. Bernard, and A. R. Robinson, 371–400. Cambridge, MA: Harvard University Press.
- Titov, V. V., and C. E. Synolakis. 1995. "Modeling of Breaking and Nonbreaking Long Wave Evolution and Runup Using VTSC-2." *Journal of Waterway, Port, Coastal and Ocean Engineering* 121 (6): 308–316. doi:10.1061/(ASCE)0733-950X(1995)121:6(308).
- Titov, V. V., and C. E. Synolakis. 1998. "Numerical Modeling of Tidal Wave Runup." *Journal of Waterway, Port, Coastal and Ocean Engineering* 124 (4): 157–171. doi:10.1061/(ASCE)0733-950X(1998)124:4(157).

- Tomita, T., K. Honda, and Y. Chida. 2016. "Numerical Simulation on Tsunami Inundation and Debris Damage STOC Model." *Report of the Port and Airport Research Institute* 55 (2): 3–33. in Japanese.
- Tomita, T., and T. Kakinuma. 2005. "Storm Surge and Tsunami Simulator in Oceans and Coastal Areas (STOC)." *Report of the Port and Airport Research Institute* 44 (2): 83–98. in Japanese.
- Tsunami Evaluation Subcommittee, Nuclear Civil Engineering Committee, Japan Society of Civil Engineers (JSCE). 2016. "Tsunami Assessment Method for Nuclear Power Plants in Japan 2016." Accessed 31 March 2021. <https://committees.jsce.or.jp/ceofnp04/tam2016en>
- Yamamoto, A., Y. Kajikawa, K. Yamashita, R. Masaya, R. Watanabe, and K. Harada. 2021. "Comparisons of Numerical Models on Formation of Sediment Deposition Induced by Tsunami Run-up." *Journal of Disaster Research* 17 (7): 1015–1029. doi:10.20965/jdr.2021.p1015.
- Yamazaki, Y., Z. Kowalik, and K. F. Cheng. 2008. "Depth-integrated, Non-hydrostatic Model for Wave Breaking and Run-up." *International Journal for Numerical Methods in Fluids* 61 (5): 473–497. doi:10.1002/flid.1952.
- Yasuda, T., K. Imai, Y. Shigihara, T. Arikawa, T. Baba, N. Chikasada, Y. Eguchi, et al. 2021. "Numerical Simulation on Detailed Urban Inundation Processes and Their Hydraulic Quantities - Tsunami Analysis Hackathon Theme 1." *Journal of Disaster Research* 17 (7): 978–993. doi:10.20965/jdr.2021.p0978.